Abelian two-Higgs model of strongly correlated electrons: Phase structure, strengthening of phase transition, and QCD at finite density

M. Bock,[1] M. N. Chernodub,[2] E.-M. Ilgenfritz,[3] and A. Schiller[1]
[1]*Institut für Theoretische Physik, Universität Leipzig, 04109 Leipzig, Germany*
[2]*ITEP, B. Cheremushkinskaya 25, 117218 Moscow, Russia*
[3]*Institut für Physik, Humboldt-Universität zu Berlin, Newtonstrasse 15, 12489 Berlin, Germany*
(Received 17 May 2007; published 2 November 2007)

We investigate nonperturbative features of a three-dimensional Abelian Higgs model with singly and doubly charged scalar fields coupled to a single compact Abelian gauge field. The model is pretending to describe various planar systems of strongly correlated electrons such as high-T_c superconductivity in the overdoped regime and exotic materials possessing excitations with fractionalized quantum numbers. The complicated phase structure of the model is studied thoroughly using numerical tools and analytical arguments. In the three-dimensional space of coupling parameters we identify the Fermi liquid, the spin gap, the superconductor and the strange metallic phases. The behavior of three kinds of topological defects—holon, spinon vortices, and monopoles—is explored in various phases. We also observe an effect, the strong enhancement of the phase transition strength reflected in a lower order of the transition: at sufficiently strong gauge coupling the two second-order phase transitions—corresponding to spinon pair and holon condensation lines—join partially in the phase diagram and become a first-order phase transition in that region. The last observation may have an analog in quantum chromodynamics at nonzero temperature and finite baryon density. We argue that at sufficiently large baryon density the finite-temperature transition between the (three-flavor paired) color superconducting phase and the quark-gluon plasma phases should be much stronger compared with the transition between two-flavor paired and three-flavor paired superconducting phases.

DOI: 10.1103/PhysRevB.76.184502 PACS number(s): 74.10.+v, 71.10.Hf, 11.15.Ha, 12.38.Aw

I. INTRODUCTION

Gauge models involving multiple scalar fields coupled to an Abelian gauge field are applicable to a large variety of systems such as multiband superconductors,[1] liquid metallic hydrogen,[2] easy-plane quantum antiferromagnets,[3] etc. These models have interesting phase structure and are distinguished by a copious zoo of topological defects. Usually, all scalar (Higgs) fields in these models are considered to be alike so that they are all equally charged and minimally coupled to the gauge field. Contrary, in this paper we consider the two-Higgs model with a gauge field and two Higgs fields with unequal charges. Our study is motivated by the fact that the charge-asymmetric two-Higgs gauge model can emerge as an effective description of unconventional superconductivity.[4]

Despite the fact that the two-Higgs model is formulated in a very simple way, it can actually capture basic properties of various systems: instanton (monopole) plasma described by the compact Abelian gauge model, superfluidity (the *XY* spin model), the $\mathbb{Z}_2$-gauge model which has analogs in particle physics, and the coupled $\mathbb{Z}_2$-gauge-*XY* model describing fractionally charged excitations in strongly correlated electron systems. It shares also a similarity with a Ginzburg-Landau model with two vector fields[5] which was suggested to describe extended *s*- and *d*-wave superconducting granular systems.

The common feature of all unconventional superconductors[6] with high critical temperatures is the presence of copper oxide layers. The layered structure is seen both in electronic[7] and optical[8] anisotropic structure of the cuprates. The anisotropy is a key ingredient of various approaches to this phenomenon.[4] The CuO_2 layers are associated with conductance plates while the atoms in the space between the layers form a so-called charge reservoir which supplies the charge carriers to the planes. The charge reservoirs themselves are almost insulating in the superconducting phase.[8] The charge carriers can be either electrons or holes depending on the nature of the dopant. The fraction of the carriers p in the planes is controlled by the doping level x which is usually encoded in the chemical formula of the cuprate oxides (i.e., $p=x$ in the structurally simple $La_{2-x}Sr_x$ CuO_4 as a prototype of many of the cuprate materials). In the clean limit, $x=0$, the cuprates are Mott insulators, while at certain x the cuprate becomes a poor conductor which—at low enough temperature—turns into a superconductor. Nowadays, the critical temperatures have climbed to the level of 140 K in Hg-based cuprates.

We concentrate on the in-plane mechanism of the high-T_c superconductivity restricting ourselves to the slave-boson approach in the *t-J* model. That model is used to describe the ground state of the high-T_c superconductor[9–11] as charge carriers (electrons or holes) in the two-dimensional copper-oxide plane. The *t-J* Hamiltonian[9] describes hopping holes (or electrons) and localized spins in a plane:

$$H_{tJ} = -t \sum_{\langle ij \rangle, \sigma} c_{i\sigma}^{\dagger} P_{ij,-\sigma} c_{j\sigma} + J \sum_{\langle ij \rangle} \left(\vec{S}_i \vec{S}_j - \tfrac{1}{4} n_i n_j \right). \qquad (1)$$

The first term specifies holes (electrons) moving without flipping the spin σ. Double occupancy is explicitly forbidden by the presence of the projectors

$$P_{ij,\sigma} = (1 - n_{i,\sigma})(1 - n_{j,\sigma}).$$

The second term describes the antiferromagnetic Heisenberg coupling between spins located at the copper sites. Here

$$\vec{S}_i = \frac{1}{2}\sum_{\sigma\sigma'} c^\dagger_{i\sigma}\vec{\tau}_{\sigma\sigma'}c_{i\sigma'}$$

is the spin operator, $c^\dagger_{i\sigma}$, $c_{i\sigma}$ are the hole (or electron) creation and annihilation operators, and

$$n_{i,\sigma} = c^\dagger_{i\sigma}c_{i\sigma}, \quad n_i = n_{i,\uparrow} + n_{i,\downarrow}$$

denotes the occupation numbers.

According to a popular scenario,[10] the electron degree of freedom can be split into the spin and charge constituents (spinon and holon, respectively). The splitting gives rise to an internal gauge degree of freedom, with respect to which the spinons and holons have positive and negative charges (say, +1 and −1, respectively). The internal group is necessarily compact and this leads to a specific interaction between the spin-charge separated constituents to be discussed later.

Under certain conditions the spinon particles become paired and form pairs similar to Cooper pairs in ordinary superconductivity. Then the pairs of spinons are presented by a spinon-pair field which has charge +2 with respect to the internal group. Therefore, in a mean-field approach, the system is described by two scalar (Higgs) fields: the holon and the spinon-pair field with internal charges −1 and +2, respectively. Both kinds of fields interact via the exchange of an internal gauge field which is compact by construction.

It is important to note that the group for the internal gauge degree of freedom has nothing to do with the usual Maxwell electromagnetic group. For example, the internal degree is compact while the electromagnetism is described by a noncompact Abelian group. The original spinon is an electromagnetically neutral excitation while the holon is the only constituent which carries the electric charge. Thus the charge carrier is the holon while the spinon may affect the properties of the strongly correlated material only indirectly: the formed spinon-pairs interact via the compact gauge field with the holons.

Entering a more technical description, the creation operators are decomposed as[10,11]

$$c^\dagger_{i\sigma} = f^\dagger_{i\sigma}b_i, \tag{2}$$

with the constraint

$$f^\dagger_{i\uparrow}f_{i\uparrow} + f^\dagger_{i\downarrow}f_{i\downarrow} + b^\dagger_i b_i = 1. \tag{3}$$

Here $f_{i\sigma}$ is a spin-particle ("spinon") operator and b_i a charge-particle ("holon") operator.

In addition to the ordinary electromagnetic (external) gauge symmetry,

$$\mathrm{U(1)_{ext}}\colon\ c_{i\sigma} \to e^{i\omega}c_{i\sigma}, \quad f_{i\sigma} \to f_{i\sigma}, \quad b_i \to e^{i\omega_i}b_i, \tag{4}$$

the spin-charge separation naturally introduces an (internal) compact U(1) gauge freedom,

$$\mathrm{U(1)_{int}}\colon\ c_{i\sigma} \to c_{i\sigma}, \quad f_{i\sigma} \to e^{i\alpha_i}f_{i\sigma}, \quad b_i \to e^{i\alpha_i}b_i, \tag{5}$$

which plays an essential role[12,13] in understanding the physics of strongly correlated electrons. The spin-charge separation idea may also be applied to various systems including the general case of nonrelativistic electrons[14] as well as the case of strongly interacting gluons in quantum chromodynamics.[15]

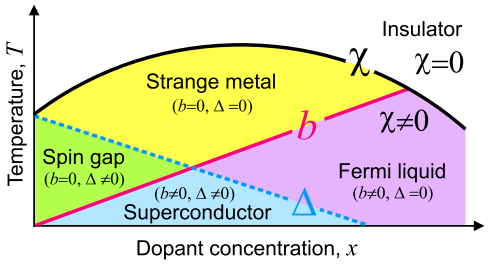

FIG. 1. (Color online) The phase diagram in the plane "temperature-dopant concentration" (suggested in Ref. 16).

The effective theory of superconductivity can further be simplified and reformulated in terms of lattice gauge models,[12,13,16–18] see recent reviews.[19] Thus, the *t*-*J* model (1) is related to a compact Abelian gauge model with the internal symmetry (5), which couples holons and spinons. As in usual BCS superconductivity, under appropriate conditions the spinons couple and form bosonic quasiparticles. In a mean-field theory one can define fields which behave under the gauge transformations (5) as

$$\chi_{ij} = \sum_\sigma \langle f^\dagger_{i\sigma}f_{j\sigma}\rangle \to \chi_{ij}e^{-i(\alpha_i-\alpha_j)}, \tag{6}$$

$$\Delta_{ij} = \langle f_{i\uparrow}f_{j\downarrow} - f_{i\downarrow}f_{j\uparrow}\rangle \to \Delta_{ij}e^{i(\alpha_i+\alpha_j)}. \tag{7}$$

The phase of the field χ represents nothing but the compact U(1) gauge field,

$$\theta_{ij} \equiv \arg\chi_{ij} \to \theta_{ij} + (d\alpha)_{ij},$$

with $(d\alpha)_{ij}=\alpha_j-\alpha_i$, and the radial part, $\chi=|\langle\chi_{ij}\rangle|$, is the so-called "resonating valence bond" (RVB) coupling. The doubly charged spinon-pair field Δ is analogous to the Cooper pair.

At high temperature the RVB coupling vanishes, $\chi=0$, and the system is in the Mott insulator (or "poor metallic") phase. With decreasing temperature χ acquires a nonzero value, eventually enabling the formation of a spinon-pair condensate $\Delta=|\langle\Delta_{ij}\rangle|$ and/or of a holon condensate $b=\langle b_i\rangle$.[11] Therefore, the following four phases[16–18] may emerge (see Fig. 1):

(i) The Fermi liquid (FL) phase with $b\neq 0$, $\Delta=0$.
(ii) The spin gap (SG) phase with $b=0$, $\Delta\neq 0$.
(iii) The superconductor (SC) phase with $b\neq 0$, $\Delta\neq 0$.
(iv) The strange metallic (SM) phase with $b=0$, $\Delta=0$.

The ground state of the superconducting layer is proposed[16,17] to be described by a compact Abelian two-Higgs model (cA2HM) in *three* dimensions with a U(1) gauge link field θ, a singly charged ($q_h=1$) holon field Φ_h, and a doubly charged ($q_s=2$) spinon-pair field Φ_s. More precisely, the classical three-dimensional (3D) statistical model describes the ground state of the zero temperature *two*-dimensional spin-charge separated quantum system of holons and spinons coupled together by the internal compact gauge field. The model can be considered as a phenomenological

extension of the Ginzburg-Landau model for ordinary low-T_c superconductors.

The model is applicable to the overdoped regime of high-T_c materials (called sometimes the SM region[4,20]) where the SU(2) particle-hole symmetry is explicitly broken. Further arguments for justifying this approach and a discussion of its limitations can be found in Ref. 4.

Since high-T_c materials are type-2 superconductors, we restrict ourselves to the London limit in which the radial parts of both Higgs fields $\Phi_k=|\Phi_k|e^{i\varphi_k}$, $k=h,s$ are frozen, $|\Phi_{h,s}|=$const. The action of this compact Abelian two-Higgs model is

$$S_{\mathrm{cA2HM}}=-\beta\sum_P \cos\theta_P-\kappa_h\sum_l \cos(d\varphi_h+\theta)_l - \kappa_s\sum_l \cos(d\varphi_s+2\theta)_l, \tag{8}$$

where $\theta_P\equiv(d\theta)_P$ is the standard lattice plaquette.

The model (8) obeys a lattice version of the U(1) internal gauge symmetry (5):

$$\theta\to\theta+d\alpha,\quad \varphi_k\to\varphi_k-q_k\alpha, \tag{9}$$

with $k=h,s$. It describes the hole (electron) "constituents" by the dynamical holon φ_h and spinon φ_s phases, which strongly interact via the dynamical gauge field θ. The inverse gauge coupling β in Eq. (8), $\beta=\chi_f+\chi_b$, is given by the diamagnetic susceptibilities χ_f of the spinon and χ_b of the holon fields. The hopping parameters κ_k are connected to the doping concentration x and the couplings t and J of Eq. (1) as follows: $\kappa_h\propto tx$ and $\kappa_s\propto J$ [see Ref. 4].

The phase diagram of the model (8) and the basic properties of the topological defects were studied for a limited set of coupling parameters in our preliminary investigation.[21] The aim of the present paper is to extend the study to a much larger coupling range using both numerical and analytical tools. We also identify the order of various phase transitions and confirm the existence of a phase transition strengthening effect which was first suggested in Ref. 21. The enhancement is reflected in decreasing the order of the phase transition at a common joint segment of two second-order transitions. The signatures of unexpected strengthening of the phase transition were later observed in a different model describing a gauge field coupled to two Higgs fields of equal charges.[22]

The structure of the paper is as follows. In Sec. II we show that the model contains three types of topological defects: two types of vortices and one type of monopole. We discuss the simplest features of the topological defects and derive their effective action using analytical tools only. In Sec. III we describe the phase diagram of the model in the three-dimensional space of gauge, holon, and spinon couplings using known results available for less complicated systems. The limiting cases of the three-dimensional phase cube are analyzed in detail and the possible structure of the phase transition surfaces in the 3D-coupling space is pointed out. Section IV is devoted to a numerical investigation of the phase diagram by Monte Carlo simulations. We analyze various two-dimensional cross sections of the 3D-phase diagram identifying numerically the order of the phase transitions. The behavior of thermodynamical quantities in combination with that of the densities of the topological defects allows us to identify the nature of the phases in different regions of the 3D-coupling space. In the same section we confirm the effect of the phase transition strengthening due to merging transition lines. The phase transition enhancement may also be relevant for quantum chromodynamics which describes the theory of strong interactions. We point out in Sec. V that the phase diagrams of the cA2HM and QCD contain common features including the joining of transition lines. We suggest that QCD at high temperature and high baryon density may experience the same strengthening effect. The last section is devoted to our conclusions.

II. PROPERTIES OF TOPOLOGICAL DEFECTS

The model (8) contains three kinds of topological defects: a monopole and two types of vortices, referred to as the holon and the spinon vortex.[4,16] The monopole has magnetic charge $2\pi\hbar$ while the holon (spinon) vortex carries magnetic flux quanta $2\pi\hbar$ ($\pi\hbar$) of the gauge field θ. One monopole is simultaneously a source of one holon vortex and two spinon vortices. In this section we discuss some basic properties of these defects.

Despite the formulation of model (8) in the Wilson representation (with an action of cosine type), the basic properties of the topological defects can be guessed from the so-called Villain representation[23] which is more suitable for analytical considerations. A similar set of transformations was performed in a noncompact model in Ref. 1. The principal difference between the compact (considered here) and noncompact models[1] is the presence of monopoles, and, as a consequence, a richer phase diagram due to the existence of confining phases.

The Villain representation of the partition function of the model (8) is

$$\mathcal{Z}=\int_{-\pi}^{\pi}D\theta\sum_{n\in\mathbb{Z}(c_2)}\int_{-\pi}^{\pi}D\varphi_h\int_{-\pi}^{\pi}D\varphi_s\sum_{l_h\in\mathbb{Z}(c_1)}\sum_{l_s\in\mathbb{Z}(c_1)} \times\exp\{-\beta\|d\theta+2\pi n\|^2-\tilde{\kappa}_h\|d\varphi_h+\theta+2\pi l_h\|^2 -\tilde{\kappa}_s\|d\varphi_s+2\theta+2\pi l_s\|^2\}, \tag{10}$$

where the Villain couplings $\tilde{\kappa}_h$ and $\tilde{\kappa}_s$ correspond to the Wilson couplings κ_h and κ_s. There are three integer-valued forms: the plaquette form n and two link forms l_h and l_s.

The definition (10) is written in a convenient condensed form by means of differential forms on the lattice.[24] In brief, the notations are as follows. Let a and b be two r forms on the lattice. Here $r=0$ corresponds to scalars (with the support on sites, c_0), $r=1$ corresponds to vectors (with the support on links, c_1), etc. Then the scalar product (a,b) is defined as a scalar product over the whole support of the r form (sites, links, etc.) over the lattice. Thus, for two vector forms ("one form"), we have $(a,b)=\Sigma_l a_l b_l$. The modulus squared is then defined as $\|a\|^2\equiv(a,a)$. The finite-difference operator "d" increases the rank of the form by one, $r\to r+1$ (thus having the meaning of a gradient), while the operator $\delta\equiv{}^*d^*$ (to be used below) decreases the rank of the form, $r\to r-1$ (having the

meaning of a divergence). The duality operator—which switches forms between the original and the dual lattices (by elementwise equating the values assigned to the dual to each other supports)—is denoted as "*."

The Berezinsky-Kosterlitz-Thouless (BKT) transformation[25] allows us to rewrite the partition function (10) in terms of monopoles and vortices. The monopoles appear due to the compactness of the gauge fields θ, and two types of vortices arise from the presence of two independent species of Higgs fields. The monopole "trajectory" (in 3D actually located on cubes) is denoted as j, the vortex "trajectory" (in 3D located on plaquettes) are σ_h (the holon vortex) and σ_s (the spinon vortex). Using the standard approach we represent the integer-valued form n as a sum $n=dq+m[j]$ of the coclosed surface dq and the surface $m[j]$ spanned on the monopole trajectory j: ${}^*j={}^*\delta m[j]$, or, equivalently, $j=dm[j]$. The two-form n can also be represented in Hodge–de Rham form as a sum of a closed and a coclosed part

$$n = \delta\Delta^{-1}j + d(\Delta^{-1}\delta m[j] + s), \tag{11}$$

where $\Delta=d\delta+\delta d$ is the lattice Laplace operator, Δ^{-1} is its inverse, and $s\in\mathbb{Z}(c_1)$, $m\in\mathbb{Z}(c_2)$, and $j\in\mathbb{Z}(c_3)$ are integer-valued forms. The monopole current is closed

$$\delta^* j = 0. \tag{12}$$

Substituting Eq. (11) into the first term under the exponent in Eq. (10) we obtain

$$d\theta + 2\pi n = dA + 2\pi\delta\Delta^{-1}j, \tag{13}$$

where

$$A = \theta + 2\pi(\Delta^{-1}\delta m[j] + s) \tag{14}$$

is a noncompact gauge field.

The same trick can be performed with the phases φ_h and φ_s [in the second and the third term in the exponent in Eq. (10)]

$$l_k = \delta\Delta^{-1}\sigma_k^{(0)} + d(\Delta^{-1}\delta p_k[\sigma_k^{(0)}] + r_k), \tag{15}$$

where $\sigma_k^{(0)}\in\mathbb{Z}(c_2)$ is the *closed* part of the holon (if $k=h$) or spinon (if $k=s$) vortex trajectory,

$$\delta^*\sigma_k^{(0)} \in \mathbb{Z}(c_2) = 0, \quad k = h,s, \tag{16}$$

$p_k\in\mathbb{Z}(c_2)$, and $r_k\in\mathbb{Z}(c_0)$. The analog of Eq. (13) can be written in the following form:

$$d\varphi_k + q_k\theta + 2\pi l_k = d\varphi_k^{\text{n.c.}} + q_k A + 2\pi\delta\Delta^{-1}\sigma_k. \tag{17}$$

Here the vortex trajectories are given by the combinations

$$\sigma_k = \sigma_k^{(0)} - q_k m[j], \tag{18}$$

and the noncompact Higgs phases are

$$\varphi_k^{\text{n.c.}} = \varphi_k + 2\pi(\Delta^{-1}\delta p_k[\sigma_k^{(0)}] + r_k). \tag{19}$$

The vortex trajectories end on the monopole "trajectories," which are points (instantons) in three-dimensional space-time,

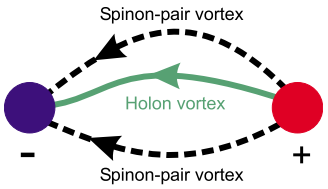

FIG. 2. (Color online) An example of a monopole-vortex configuration.

$$\delta^*\sigma_k + q_k{}^*j = 0, \quad k = h,s. \tag{20}$$

The above equation means that there is one holon vortex and two spinon vortices—each carrying a corresponding elementary flux—attached simultaneously to each monopole. A typical configuration monopole-vortex configuration is shown in Fig. 2.

Substituting Eqs. (13) and (17) into Eq. (10) and performing the Gaussian integration over the noncompact fields A, $\varphi_h^{\text{n.c.}}$, and $\varphi_s^{\text{n.c.}}$, one obtains the BKT representation of the two-Higgs model,

$$\mathcal{Z} = \sum_{{}^*j\in\mathbb{Z}({}^*c_3)} \sum_{{}^*\sigma_{h,s}\in\mathbb{Z}({}^*c_2)} e^{-S^{\text{mon}}[j]-S^{\text{vort}}[\sigma_h,\sigma_s]}, \tag{21}$$
$$\delta^*\sigma_k+q_k{}^*j=0$$

where an irrelevant constant factor is omitted. The monopole and the vortex actions are, respectively,

$$S^{\text{mon}}[j] = 4\pi^2\beta\left(j, \frac{1}{\Delta + m_\gamma^2}j\right), \tag{22}$$

$$S^{\text{vort}}[\sigma_h,\sigma_s] = 4\pi^2 \sum_{k,k'=h,s} (\sigma_k, \mathcal{K}_{kk'}\sigma_{k'}), \tag{23}$$

with the differential operator $\mathcal{K}$,

$$\mathcal{K}_{kk'} = \frac{\tilde{\kappa}_k}{\Delta}\left(\delta_{kk'} - \frac{q_k}{q_{k'}}\frac{\omega_{k'}m_\gamma^2}{\Delta + m_\gamma^2}\right). \tag{24}$$

In Eqs. (22) and (24) m_γ denotes the mass of the photon,

$$m_\gamma^2 = \frac{1}{\beta}(\tilde{\kappa}_h + 4\tilde{\kappa}_s), \tag{25}$$

and ω_k are the normalized weights

$$\omega_k = \frac{q_k^2\tilde{\kappa}_k}{\tilde{\kappa}_h + 4\tilde{\kappa}_s}, \quad \omega_h + \omega_s = 1. \tag{26}$$

The (self-)interaction of the monopoles and vortices can readily be read off from Eqs. (21)–(23). The monopoles interact via a massive photon exchange, and thus the interactions of the monopole "trajectories" are suppressed at large distances.

The vortex interactions contain a long-range term. The origin of the long-range forces is simple: in the Abelian model with one Higgs field the massless Goldstone mode is eaten up by the longitudinal component of the gauge field. Thus, the gauge field becomes massive, whereas the massless Goldstone boson disappears. This is not the case in the

present model with two Higgs fields: one of the Goldstone bosons can be absorbed into the longitudinal component of the gauge field, while the other remains alive. Thus, the two-Higgs system with one gauge field will always have one massless excitation which, in particular, leads to a long-range interaction between the vortex "surfaces."

The vortex-vortex interaction term [Eqs. (23) and (24)] also be rewritten in the form

$$S^{\mathrm{vort}}[\sigma_h,\sigma_s] = S^{\mathrm{vort}}_{hh}[\sigma_h] + S^{\mathrm{vort}}_{ss}[\sigma_s] + S^{\mathrm{vort}}_{sh}[\sigma_h,\sigma_s] \quad (27)$$

where the holon-holon, spinon-spinon, and holon-spinon vortex interactions are, respectively,

$$S^{\mathrm{vort}}_{hh} = 4\pi^2\tilde{\kappa}_h\left(\sigma_h,\left[\omega_h\frac{1}{\Delta+m_\gamma^2}+\omega_s\frac{1}{\Delta}\right]\sigma_h\right), \quad (28)$$

$$S^{\mathrm{vort}}_{ss} = 4\pi^2\tilde{\kappa}_s\left(\sigma_s,\left[\omega_s\frac{1}{\Delta+m_\gamma^2}+\omega_h\frac{1}{\Delta}\right]\sigma_s\right), \quad (29)$$

$$S^{\mathrm{vort}}_{hs} = 8\pi^2(\tilde{\kappa}_h\tilde{\kappa}_s\omega_h\omega_s)^{1/2}\left(\sigma_h,\left[\frac{1}{\Delta+m_\gamma^2}-\frac{1}{\Delta}\right]\sigma_s\right). \quad (30)$$

From these expressions it can be seen that the short-range interaction between the parallel segments of all vortices is always repulsive. However, the presence of the long-range component acts in a different way: segments of equal type vortices are repulsive (holon-holon and spinon-spinon), while the parallel vortex segments of different types (holon-spinon) are always attractive. The respective strengths of the repulsion and attraction depend on the weights of the holon and spinon vortices, Eq. (26), which, in turn, depend on the strengths of the holon and spinon-pair condensates, $\tilde{\kappa}_k \propto |\Phi_k|^2$.

The presence of the massless mode in the interaction between vortices (28)–(30) on the Lagrangian level does not mean that on the quantum level the interactions remain unscreened. On the contrary, we expect that the massless mode should disappear due to nonperturbative effects. This happens, for example, in the monopole gas of the three-dimensional compact Abelian model.[26] Indeed, in this example the bare interaction between the monopoles is of the Coulomb type, $(j,\Delta^{-1}j)$, while all correlations in the statistical ensembles of the monopoles are exponentially suppressed at large distances by a Debye mass which appears due to monopole interactions in the plasma regime. A similar effect is expected in the considered system of Coulomb-interacting vortices. In the dilute ensemble of vortices the screening mass is expected to be small compared to the mass of the photon m_γ, Eq. (25), but still nonzero. Therefore one may expect that on the quantum level the Goldstone mode may disappear.

III. THE PHASE DIAGRAM

The internal structure of the three-dimensional phase diagram of the (London limit version of the) compact Abelian two-Higgs model (8) is rather complicated. However, the faces and the edges of the cube representing the "compactified" phase diagrams can be drawn relatively easily because they are related to various well-known condensed-matter systems. These limiting cases of the phase cube correspond to appropriate combinations of vanishing and/or infinitely large couplings β, κ_h, and κ_s. Below we discuss these limits in detail.

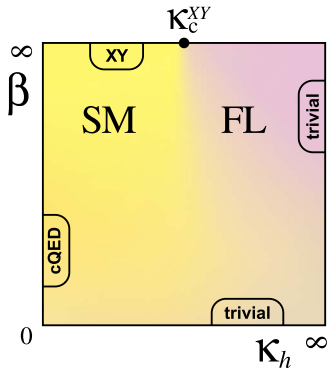

FIG. 3. (Color online) The phase diagram on the $\kappa_s=0$ face corresponds to the compact Abelian $Q=1$ Higgs model with the action (31). The SM and FL phases in the interior of the diagram, as well as the limiting models (XY, cQED, and the trivial cases) are explicitly indicated. The XY critical point is given in Eq. (34).

A. The (β,κ_h) faces

The κ_s parameter defines the coupling of the spinon-pair field to the compact gauge field. Below we consider two limiting cases corresponding to vanishing and infinitely strong coupling κ_s.

1. The $\kappa_s=0$ face: $Q=1$ compact Abelian Higgs model

The $\kappa_s=0$ face of the cA2HM corresponds to the $Q=1$ Higgs model with a compact Abelian field ($\mathrm{cAHM}_{Q=1}$) in three dimensions:

$$S_{\mathrm{cAHM}_{Q=1}} = -\beta\sum_P \cos\theta_P - \kappa_h\sum_l \cos(d\varphi_h+\theta)_l. \quad (31)$$

On that face the holon condensate is coupled to the compact U(1) gauge field while the spinon-pair field is decoupled from all other fields. The phase of the spinon-pair field is disordered which implies condensation of the spinon vortices and, therefore, vanishing of the spinon-pair condensate Δ.

The $\mathrm{cAHM}_{Q=1}$ has extensively been studied in the literature and it seems that a consensus on the phase structure is reached.[27–30] The phase diagram in the (β,κ_h) plane is plotted in Fig. 3. It contains two phases: (i) The SM phase at small β/small κ_h and (ii) the FL phase at large β/large κ_h. The FL phase is the broken or Higgs phase with nonzero holon condensate $b\neq 0$, and the SM phase is the confining or symmetric phase with $b\approx 0$. The distinction between these phases is blurry since the broken phase is always partially confining while (at the opposite end) even in the deeply confining phase traces of the Higgs condensate can be found. The usual order parameter—the Higgs (holon) condensate—is, strictly speaking, nonzero in the whole phase diagram,

and thus it is usually said that these phases are "analytically connected." As a consequence there is no *local* order parameter in terms of the primary fields of the model, which could in principle discriminate between the phases.

Despite the boundary between broken and confining "phases" definitely not having the characteristics of a phase transition in the thermodynamic sense, these phases may be discriminated by the condensation properties of topological defects. A nonthermodynamic boundary of this type is known in the literature as a Kertész line,[31] which is defined as a line where the vortices start and/or cease to condense. This line—which is not plotted in Fig. 3—has been thoroughly studied in the three-dimensional Abelian Higgs model in Ref. 32 and was suggested to appear in models of particle physics as well.[33] Note that in the present context the word "line" refers to a two-dimensional coupling parameter space, while in, say, a three-dimensional parameter space the corresponding manifold is a surface.

The edges of the cube in the $\kappa_s=0$ plane can be analyzed following Refs. 27–30. At the $\kappa_h=0$ edge the model is basically a plasma model. In fact, along the $\kappa_h=\kappa_s=0$ edge the cA2HM reduces to the pure compact U(1) gauge theory,

$$S_{\mathrm{cQED}} = -\beta \sum_P \cos\,\theta_P, \tag{32}$$

which is known to be confining at any value of β due to the presence of monopoles.[26] The monopoles are interacting as Coulomb particles, thus forming a magnetically neutral plasma. In three dimensions the monopoles are pointlike, i.e., instantonlike objects. Along the $\kappa_h=\kappa_s=0$ edge the vacuum of the model possesses a mass gap at any nonzero density of monopoles, which is realized at any finite β. The mass gap is given by the Debye mass of the monopole plasma.

Along the edge $\beta\to\infty$, $\kappa_s=0$ the model describes a superfluid. Indeed, along this edge the gauge field becomes constrained to the trivial vacuum, $d\theta=0$. The constraint is resolved as $\theta=d\alpha$. Identifying $\alpha+\varphi_h=\varphi$, the model becomes the 3D *XY* spin model

$$S_{XY} = -\kappa^{XY} \sum_l \cos(d\varphi)_l, \tag{33}$$

where we have set $\kappa_h \equiv \kappa^{XY}$. The *XY* model is known to possess a second-order transition[34] at the critical point

$$\kappa_c^{XY} \approx 0.454\,20\ldots, \tag{34}$$

shown by the dot in Fig. 3.

The edges $\beta=0$ and $\kappa_h\to\infty$ correspond to trivial theories so that they do not possess any phase transitions.

2. The $\kappa_s\to\infty$ face: XY spins coupled to $\mathbb{Z}_2$ gauge field

In the limit $\kappa_s\to\infty$ the coupling of the spinon-pair field and the gauge field is tight. Mathematically, this is expressed in the form of the constraint

$$2\theta + d\varphi_s = 2\pi m, \quad m \in \mathbb{Z}, \tag{35}$$

which is to be fulfilled at each link. The constraint (35) has the solution $\theta=(d\varphi_s/2+\pi m)_{2\pi}$, where $m\in\mathbb{Z}$ is chosen such that $\theta\in(-\pi,\pi]$. Substituting this solution back into Eq. (8),

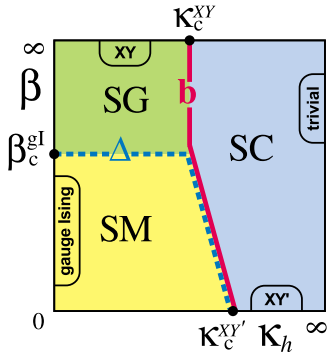

FIG. 4. (Color online) The phase diagram on the $\kappa_s\to\infty$ face corresponding to the model (36). The critical points at the edges and the phase transition lines in the interior are discussed in the text.

and introducing the $\mathbb{Z}_2$ gauge field $\sigma_l=(-1)^{m_l}$, we understand that on the face $\kappa_s\to\infty$ the model (8) reduces to a 3D *XY* $-\mathbb{Z}_2$ model with the action

$$S_{XY-\mathbb{Z}_2} = -\beta \sum_P \sigma_P - \kappa_h \sum_l \sigma_l \cos(d\varphi)_l. \tag{36}$$

This model describes a *XY*-type matter field $\varphi=\varphi_h-\varphi_s/2$ which interacts via the exchange of a $\mathbb{Z}_2$ gauge field σ_l. The model has a rich phase structure studied numerically in Ref. 35. The phase diagram—plotted in Fig. 4—contains the following three phases:

(i) The SM phase at small β/small κ_h.
(ii) The SG phase at large β/small κ_h.
(iii) The SC phase at large β/large κ_h.

As one can see from Fig. 4 the phase structure of the $\kappa_s\to\infty$ face is much richer than that of the $\kappa_s=0$ face.

Let us analyze the edges of this two-dimensional phase diagram. At the $\kappa_h=0$ edge the model is reduced to the $\mathbb{Z}_2$ gauge (or, the "gauge Ising") model[36] with the action

$$S_{\mathrm{gI}} = -\beta \sum_P \sigma_P. \tag{37}$$

This model has a string-like topological object as well as vacuum excitations which are sometimes considered as prototypes of, respectively, the chromoelectric string and glueball excitations in the strongly interacting quark systems in non-Abelian gauge theories.[37]

The gauge Ising model (37) is known to possess a second-order phase transition of the Ising type at the critical point

$$\lim_{\kappa_h\to 0} \beta_c(\kappa_h) = \beta_c^{\mathrm{gI}} \approx 0.7613\ldots \tag{38}$$

shown by the dot at $\kappa_h=0$ edge of Fig. 4. This transition separates the disordered (small β) and ordered (large β) phases discriminated by the absence or presence of the spinon-pair condensate, $\Delta=0$ and $\Delta\neq 0$, respectively. At the same time, at this axis the holon condensate vanishes due to disorder in the *XY* variables (to be discussed below). Therefore the small-β and large-β phase are identified with the SM and SG phases, respectively.

At the $\beta\to\infty$ edge the $\mathbb{Z}_2$ gauge field is suppressed due to the constraint $\sigma_P=1$, so that the model is reduced to the *XY*

model (33) with a coupling $\kappa^{XY} \equiv \kappa_h$. At small values of this coupling, $\kappa_h < \kappa_c^{XY}$, the holon field is disordered by vortices and the holon condensate is absent. At large values $\kappa_h > \kappa_c^{XY}$, the vortices are dilute and holon condensation takes place. These regimes are separated by the critical coupling (34) which is marked by the dot at the $\beta \to \infty$ edge of the phase diagram, Fig. 4.

The interior of the phase diagram is also nontrivial. The phase transitions, marking the onset of spinon-pair (dotted line) and holon (solid line) condensations, are departing from the $\kappa_h = 0$ and $\beta \to \infty$ edges towards the center of the phase diagram. There they meet together forming a single transition line where the holon and spinon-pair condensations occur simultaneously, Fig. 4. This combined line extends down to lower β, and finally it meets with the $\beta = 0$ edge of the phase diagram. It is described by a (modified) XY' model with the action

$$S_{XY'} = -\sum_l \log \cosh[\kappa_h \cos(d\varphi)_l], \tag{39}$$

which can be derived explicitly from Eq. (36). The modified XY' model (39) possesses a second-order phase transition at the critical point[35]

$$\lim_{\beta \to 0} \kappa_{h,c}(\beta) = \kappa_c^{XY'} \approx 1.6. \tag{40}$$

The $\kappa_h \to \infty$ edge is trivial, being occupied by the superconducting phase with both the holon and the spinon-pair condensates present.

The model (36) alone was supposed[38] to possess an interesting link to the physics of correlated electrons being able to describe certain exotic phases. The topological objects of this model are called "visons" which are fractionally charged excitations. In the language of the Abelian two-Higgs model the vison coincides with the spinon vortex, while the holon vortex turns into a XY vortex, φ becomes the field of the so-called "chargon" particle. The SG phase corresponds to the fractionalized phase where visons are absent and chargons are free particles. In the SM phase the visons are condensed, and chargons are confined. The SC phase corresponds to a superfluid state where both visons and XY vortices are dilute and chargons are free.

B. The (β, κ_s) faces

The coupling between the holon field and the gauge field is controlled by the parameter κ_h. Below we consider the influence of the spinons on the phase diagram considering the limits of large $(\kappa_h \to \infty)$ and small couplings $(\kappa_h \to 0)$.

1. The $\kappa_h = 0$ face: $Q=2$ compact Abelian Higgs model

On the $\kappa_h = 0$ face the holon condensate vanishes, $b \equiv 0$, and the spinon-pair condensate Δ is described by the $\mathrm{cAHM}_{Q=2}$ model

$$S_{\mathrm{cAHM}_{Q=2}} = -\beta \sum_P \cos \theta_P - \kappa_s \sum_l \cos(d\varphi_s + 2\theta)_l. \tag{41}$$

The phase diagram of this model in the (β, κ_s) plane is well known and the behavior of the spinon-pair condensate can be deduced from results of Refs. 27, 39, and 40. Before doing so, let us consider the edges of the phase diagram.

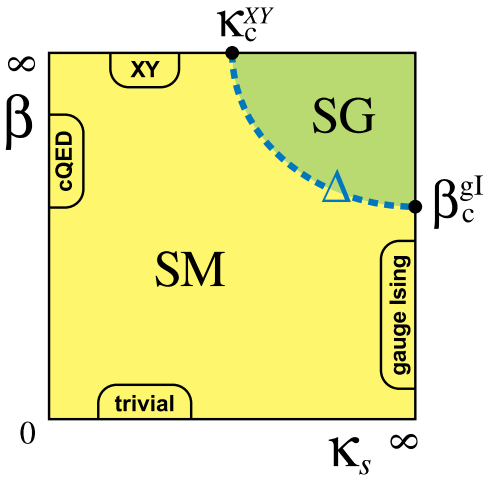

FIG. 5. (Color online) The phase diagram of the compact Abelian $Q=2$ Higgs model (41) on the $\kappa_h = 0$ face.

The edges $\kappa_s = 0$ and $\beta = 0$ do not possess any phase transitions because they are described, respectively, by the cQED model (32) and by a trivial model.

The edge $\beta \to \infty$ corresponds to the XY model, since in this limit the constraint $d\theta = 0$ is imposed. The constraint is resolved by setting $\theta = d\alpha$, with subsequent identification

$$\varphi_s + 2\alpha - 2\pi l = \varphi \in (-\pi, \pi]$$

with $l \in \mathbb{Z}$. Then we obtain the XY action (33) by setting $\kappa^{XY} \equiv \kappa_s$. The XY model describes the superfluid behavior of the spinon-pair condensate with the XY critical point (34), κ_c^{XY}.

The edge $\kappa_s \to \infty$ corresponds to the gauge Ising model (37) because in this limit the constraint

$$d\varphi_s + 2\theta = 2\pi m, \quad m \in \mathbb{Z},$$

is automatically imposed. The constraint is resolved as

$$\theta = \pi m - d\varphi_s/2 + 2\pi n, \quad n \in \mathbb{Z},$$

leading subsequently to

$$d\theta = \pi dm, \quad \cos d\theta = \cos \pi dm \equiv \sigma_P,$$

where $\sigma_l = (-1)^{m_l}$ is the $\mathbb{Z}_2$ gauge field attached to the link l. Then Eq. (41) reduces to Eq. (37), and the edge $\kappa_s \to \infty$ possesses a critical point at $\beta_c = \beta_c^{\mathrm{gI}}$ which marks the second-order phase transition of Ising type.

The critical points at the $\beta \to \infty$ and $\kappa_s \to \infty$ edges are connected by a second-order phase transition line as shown by the dotted line in Fig. 5. The SM phase is located at small β and/or small κ_s, while the SG phase is residing in the large β/large κ_s corner. The transition line corresponds to the onset of spinon-pair condensation Δ. In the whole diagram the holon condensate is absent, $b = 0$. In addition also the limiting models (XY, cQED, gauge Ising, and trivial cases) together with the critical points κ_c^{XY}, Eq. (34), and β_c^{gI}, Eq. (38), are indicated.

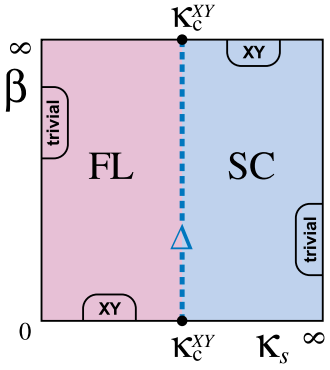

FIG. 6. (Color online) The phase diagram of the XY model (33) together with the limiting models at the edges on the $\kappa_h \to \infty$ face.

2. The $\kappa_h \to \infty$ face: XY model

On the $\kappa_h \to \infty$ face the model (8) reduces to the XY model (33) with a hopping parameter $\kappa \equiv \kappa_s$ and $\varphi = -2\varphi_h + \varphi_s$. The model controls the superfluid behavior of the spinon-pair condensate Δ. Due to the constraint

$$\theta = d\varphi_h + 2\pi l, \quad l \in \mathbb{Z},$$

the holon vortices are suppressed and therefore $b \neq 0$ in the whole (β, κ_s) plane. The phase diagram—shown in Fig. 6—is divided by a second-order XY-like transition line parallel to the β axis at $\kappa_{s,c}(\beta) = \kappa_c^{XY}$ shown as a dotted line. This line separates the FL phase (with condensed spinon vortices and $\Delta = 0$) at $\kappa_s < \kappa_c^{XY}$ from the SC phase (with suppressed spinon vortices and $\Delta \neq 0$) at $\kappa_s > \kappa_c^{XY}$. In the whole diagram the holon field is condensed, $b \neq 0$.

C. The (κ_h, κ_s) faces

Now we consider the effect of choosing the extreme limits of very strong and very weak gauge couplings, $\beta = 0$ and $\beta \to \infty$, respectively.

1. The $\beta = 0$ face: An ultralocal two-Higgs system

On the $\beta = 0$ face we obtain a two-Higgs system interacting ultralocally via a nonpropagating gauge field. The one-link action of the model is given by

$$e^{-S_l[\varphi_h, \varphi_s]} = \int D\theta \exp\left(\sum_{k=h,s} \kappa_k \cos(d\varphi_k + q_k \theta)_l \right). \quad (42)$$

In order to obtain this part of the weight for the limiting model we put $\beta = 0$ in Eq. (8) and keep the integration over the gauge field θ. We expand the two factors of the exponentiated one-link action in Eq. (42) in a Fourier series,

$$e^{\kappa_k \cos(d\varphi_k + q_k \theta)_l} = \sum_{n_k \in \mathbb{Z}} I_{n_k}(\kappa_k) e^{i[(d\varphi_k + q_k \theta)_l] n_k}, \quad (43)$$

for $q_h = 1$ and $q_s = 2$. Here $I_n(\kappa)$ is the modified Bessel function of nth order. Substituting Eq. (43) in Eq. (42) and performing the integration over θ we obtain the constraint

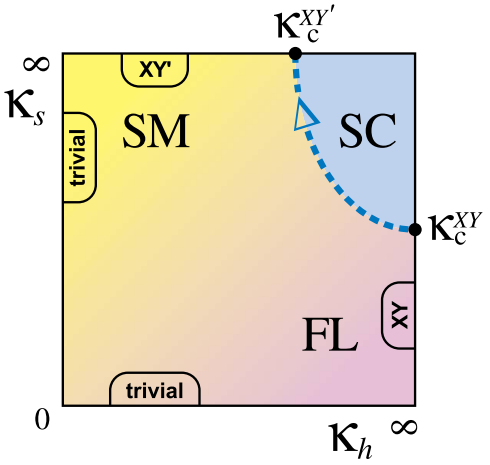

FIG. 7. (Color online) The phase diagram of the ultralocal two-Higgs system (44) on the $\beta = 0$ face.

$n_h + 2n_s = 0$. Setting $n_s = -n_h/2 = n$, we obtain (up to an inessential factor in front of the sum)

$$e^{-S_l[\varphi_h, \varphi_s]} = \sum_{n \in \mathbb{Z}} I_{2n}(\kappa_h) I_n(\kappa_s) e^{id(\varphi_s - 2\varphi_h)n}, \quad (44)$$

where we used the property $I_n \equiv I_{-n}$. Note that the quantities n, $d\varphi_h$, $d\varphi_s$ in Eq. (44) are defined at the same link l.

In the (κ_h, κ_s) plane one has two phases: the SC phase with nonzero condensates Δ and b in the large κ_h/large κ_s corner and a SM-FL phase in the remaining part of the phase diagram. The phase diagram is shown in Fig. 7. The SC and SM-FL phases are separated by a second-order XY-type phase transition (indicated by a dotted line) which starts at $\kappa_{h,c} = \kappa_c^{XY'}$, Eq. (40), at the $\kappa_s \to \infty$ edge and ends at $\kappa_{s,c} = \kappa_c^{XY}$, Eq. (39), for $\kappa_h \to \infty$. At these two edges the two-Higgs model (44) is reduced to a modified (39) and a usual (33) XY model, respectively. The SM-FL phase appears actually as the FL phase ($b \neq 0$) at large κ_h, and the SM phase ($b \to 0$) is realized at large κ_s (the structure of the SM-FL phase is plotted in Fig. 3).

2. The $\beta \to \infty$ face: Two decoupled XY models

Finally, on the $\beta \to \infty$ face the system (8) reduces to two decoupled XY models describing the holon and spinon-pair superfluids. This fact is readily seen from the partition function (8): large β imposes the constraint $d\theta = 0$ which is resolved, as usual, by $\theta = d\alpha + 2\pi n$, $n \in \mathbb{Z}$. Substituting this solution back to (8) and performing the redefinitions of the phases, $\varphi_h + \alpha \to \varphi_h$ and $\varphi_s + 2\alpha \to \varphi_s$, one obtains

$$S_{2XY} = -\kappa_h \sum_l \cos(d\varphi_h)_l - \kappa_s \sum_l \cos(d\varphi_s)_l. \quad (45)$$

The phase diagram in the (κ_h, κ_s) plane includes all discussed phases (SM, SG, SC, and FL) as shown in Fig. 8. The phases are separated by the straight solid (condensation of the holon b) and dashed (condensation of the spinon-pair Δ) phase transition lines at $\kappa_{h,c} = \kappa_c^{XY}$ and $\kappa_{s,c} = \kappa_c^{XY}$, Eq. (34), respectively.

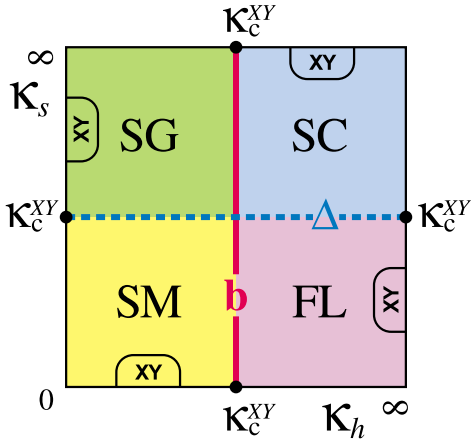

FIG. 8. (Color online) The phase diagram on the $\beta \to \infty$ face of the two decoupled XY models (45).

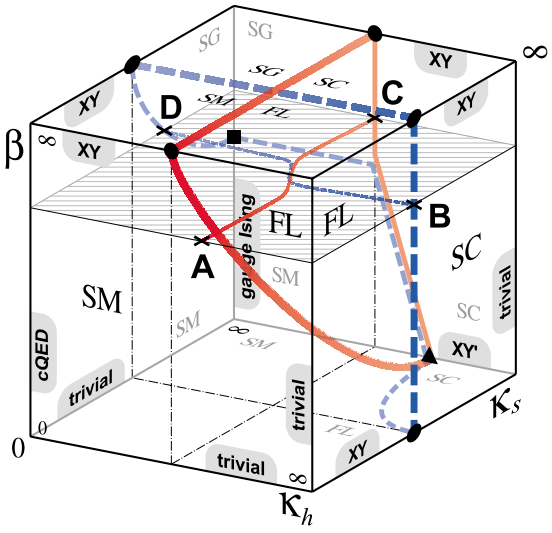

FIG. 9. (Color online) The qualitative 3D phase diagram of the cA2HM (reproduced from Ref. 21).

D. The interior of the 3D phase diagram

Knowing the limiting cases shown in Figs. 3–8 allows us (following Ref. 21) to reconstruct the interior of the three-dimensional phase diagram as shown schematically in Fig. 9. In other words, the six faces of the 3D cube, Fig. 9, correspond to the 2D diagrams plotted in Figs. 3–8.

The shaded section in Fig. 9 represents the phase diagram in the (κ_h, κ_s) plane at fixed finite gauge coupling β in the region $\beta_c^{\mathrm{gI}} < \beta < \infty$. *A priori* there are two possible views to expect of the internal section of the phase diagram. One of the options is plotted schematically in Fig. 10(a). The holon and spinon-pair condensation lines are getting slightly curved with respect to the limiting $(\beta \to \infty)$ case shown in

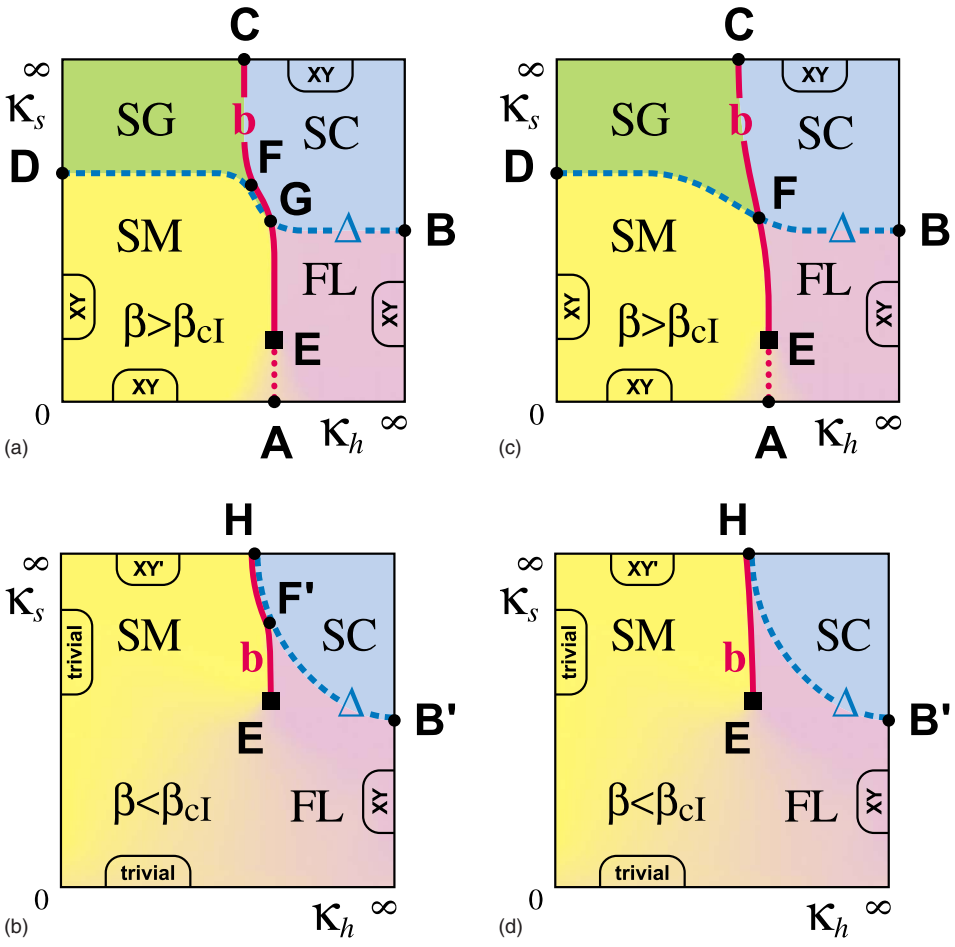

FIG. 10. (Color online) The 2D section of the 3D phase cube at a fixed gauge coupling β: (a) $\beta_c^{\mathrm{gI}} < \beta < \infty$ and (b) $0 < \beta < \beta_c^{\mathrm{gI}}$. The meaning of the points $A, B, \ldots$ is explained in the text. In both figures in the middle of the diagram the transition lines of b and Δ condensation join along a finite segment. (c) and (d) represent the respective alternative scenario with the transition lines intersecting instead of piecewise merging together.

Fig. 8: the solid (dashed) line, which marks the condensation of the holon b (spinon-pair Δ), becomes generally shifted towards larger values of κ_h (κ_s). The holon condensation line starts at large values of κ_s at the point

$$\kappa_{h,c}(\beta) > \kappa_{h,c}(\infty) \equiv \kappa_c^{XY}.$$

This point is marked as point C in Figs. 9 and 10(a). With κ_s becoming smaller the b-condensation line meets the Δ-condensation line at point F, and they continue together until point G, at which these transition split again. Then the b-condensation line continues alone and eventually stops at an end point E in the interior of the diagram. A projection of this line to the edge $\kappa_s=0$ [marked in Fig. 10(a) by the dotted line E-A] might eventually be visible as a percolation transition. The Δ-condensation transition, denoted by the dashed line D-F-G-B, does not have an end point.

The two-dimensional section qualitatively changes as β becomes smaller than the critical coupling β_c^{gI} of the gauge Ising model. An example of such a section is shown in Fig. 10(b). At sufficiently strong gauge coupling, $\beta<\beta_c^{\mathrm{gI}}$, points C, D, and F merge together into the point denoted now as H and the SG phase pocket disappears. The b- and Δ-condensation lines begin to run together from point H until point F' [formerly point G in Fig. 10(a)] in the interior of the phase diagram, where the lines split again: the Δ-condensation goes to point B', while the b-condensation line runs towards the $\kappa_s=0$ edge but ends at a new end point E. As β decreases further, Fig. 10(b) gradually evolves into Fig. 7: at $\beta=0$ the end point E becomes finally point H. As a result, the b-condensation transition disappears completely, as it is plotted in Fig. 7.

The alternative to the above scenario—which cannot be excluded by analytical means—is represented in Figs. 10(c) and 10(d). The difference is in the mutual behavior of the b- and Δ-condensation lines in the interior of the phase diagram. In Fig. 10(a) these transitions piecewise join along a common segment F-G. In Fig. 10(b) the common segment is H-F'. The alternative of Fig. 10(a) is plotted in Fig. 10(c): Instead of merging along the F-G segment the transition lines intersect in point F. The alternative of Fig. 10(b) is plotted in Fig. 10(d): instead of having the common segment H-F' [in Fig. 10(b)] the b- and Δ-transition lines have only a common starting point H and separate immediately.

To discriminate between these scenarios numerical simulations have to be used. This is presented in the next section.

IV. NUMERICAL RESULTS

A. Observables

In order to clarify the structure of the phase diagram we have performed a numerical study of various gauge-invariant quantities. One potentially sensitive quantity is the action of the model, or any (gauge-invariant) part of it. This fact is easy to understand since the action governs the dynamics of the whole model. Using a familiar notation, the action of our lattice model is given as

$$S = -\beta S_P - \kappa_h S_h - \kappa_s S_s \tag{46}$$

with

$$S_P = \sum_{x,\mu<\nu} \cos(\theta_{x,\mu} + \theta_{x+\hat{\mu},\nu} - \theta_{x+\hat{\nu},\mu} - \theta_{x.\nu}),$$

$$S_h = \sum_{x,\mu} \cos[\varphi_h(x+\hat{\mu}) - \varphi_h(x) + \theta_{x,\mu}],$$

$$S_s = \sum_{x,\mu} \cos[\varphi_s(x+\hat{\mu}) - \varphi_s(x) + 2\theta_{x,\mu}]. \tag{47}$$

Here x denotes the sites of the 3D lattice, nearest neighbors are separated by a lattice spacing a, and $\hat{\mu}$ is the shift vector in the μ direction. The compact lattice gauge field angles $\theta_\mu(x) \in (-\pi, \pi]$ live on the links (bonds) between sites x and $x+\hat{\mu}$, the holon fields $\varphi_h(x)$ (phase angles of a singly charged scalar field) and the spinon-pair fields $\varphi_s(x)$ (phase angles of a doubly charged scalar field) are defined on the sites. The coupling $\beta=1/g^2$ is the inverse gauge coupling squared, and κ_h and κ_s express the coupling between Higgs and gauge fields, respectively. In the following κ_h and κ_s are called "hopping parameters." To study this model by means of Monte Carlo we use standard Metropolis updates for all three kinds of fields.

In order to characterize the different phases of the model we consider the following "thermodynamical" expectation values (related to the derivatives of the logarithm of the partition function with respect to the couplings):

$$\langle E_P \rangle = \left\langle \frac{1}{N_P} S_P \right\rangle,$$

$$\langle E_h \rangle = \left\langle \frac{1}{N_L} S_h \right\rangle,$$

$$\langle E_s \rangle = \left\langle \frac{1}{N_L} S_s \right\rangle, \tag{48}$$

called plaquette, holon link, and spinon link expectation values. Here $N_{P/L/S}$ is the number of plaquettes and/or links and/or sites on the finite lattice ($N_P=N_L$ in three dimensions), $\langle \cdots \rangle$ denotes the ensemble average over configurations. In addition, the susceptibilities of these quantities (related to the second derivatives of the logarithm of the partition function with respect to the couplings) have been considered:

$$\chi_{E_P} = N_P(\langle E_P^2 \rangle - \langle E_P \rangle^2),$$

$$\chi_{E_{h,s}} = N_L(\langle E_{h,s}^2 \rangle - \langle E_{h,s} \rangle^2). \tag{49}$$

The simplest characteristics of a topological defect is its density. Using the notations of Sec. II the monopole and the vortex densities are defined as, respectively,

$$\rho_{\mathrm{mon}} = \frac{1}{N_S} \sum_{^*c_3} |{}^*j|, \quad \rho_{h,s} = \frac{1}{N_L} \sum_{^*c_2} |{}^*\sigma_{h,s}|. \tag{50}$$

Here ${}^*c_3$ are the sites of the dual lattice dual to the cubes of the original lattice, and ${}^*c_2$ are the links of the dual lattice dual to the plaquettes of the original lattice. The monopole charge is defined in the standard way,

$$j = \frac{1}{2\pi} d[d\theta]_{2\pi}, \tag{51}$$

where $[\cdots]_{2\pi}/(2\pi)$ denotes the integer part modulo 2π. Note that the plaquette angle $d\theta$ lies in the range $-\pi$ to π plus or minus integer multiples of 2π. Thus, effectively using the Gauss's law, one considers a forward cube from a lattice position x built up by six plaquettes, defines the integer-valued so-called oriented Dirac strings n passing through these plaquettes and sums over these integers assigned to the outward pointing oriented strings. This sum defines the monopole number in the cube corresponding to a point of the dual lattice. Following Ref. 41, the holon and spinon vortex currents are defined as

$$\sigma_k = \frac{1}{2\pi}(d[d\varphi + q_k\theta]_{2\pi} - q_k[d\theta]_{2\pi}), \quad k = h,s. \tag{52}$$

These integer-valued oriented currents pierce a given plaquette corresponding to a link of the dual lattice. Together with ρ_{mon} and $\rho_{h,s}$ we measure also the corresponding susceptibilities

$$\chi_{\rho_{\mathrm{mon}}} = N_S(\langle \rho_{\mathrm{mon}}^2 \rangle - \langle \rho_{\mathrm{mon}} \rangle^2),$$

$$\chi_{\rho_{h,s}} = N_L(\langle \rho_{h,s}^2 \rangle - \langle \rho_{h,s} \rangle^2). \tag{53}$$

In this section we report on Monte Carlo studies of the phase transitions within two-dimensional cross sections of the whole phase diagram characterized by certain fixed values of the (inverse) gauge coupling β. These planes are parametrized by the two hopping parameters κ_h and κ_s.

It is important to note that we have to distinguish between the cross sections lying above and below the critical value $\beta_c^{\mathrm{gI}} \approx 0.7613$, corresponding to the phase transition of the pure gauge Ising model. As we have discussed above, the qualitative structure of the phase diagram is different above and below this phase transition, obtained by moving the shaded square in Fig. 9 up and down. The SG phase (the phase with zero holon condensate and nonzero spinon-pair condensate) is absent in the $\beta < \beta_c^{\mathrm{gI}}$ (strong gauge coupling) region contrary to the $\beta > \beta_c^{\mathrm{gI}}$ (weak gauge coupling) part of the phase diagram.

In our previous work[21] we restricted ourselves to the larger β region and presented results mainly for $\beta = 1.0$. In order to obtain the gross features of the different phases, we perform the initial studies on 16^3 lattices, focusing at different fixed values of β. Based on the expectations as described in the previous Sec. III, we have used a dense grid of points spanning the (κ_h, κ_s) hopping parameter plane over a range where we expect a nontrivial behavior of the model.

B. Phase structure at weak gauge coupling

According to our analysis presented above, in the weak coupling region, $\beta > \beta_c^{\mathrm{gI}}$, the phase diagram contains all four phases. The summary of our results on the phase structure of the model is presented in Figs. 11–13. These figures show the two-dimensional cross sections—explored, respectively, at $\beta = 2.0$, $\beta = 1.5$, and $\beta = 1.0$ values of the gauge coupling—of the full three-dimensional phase diagram.

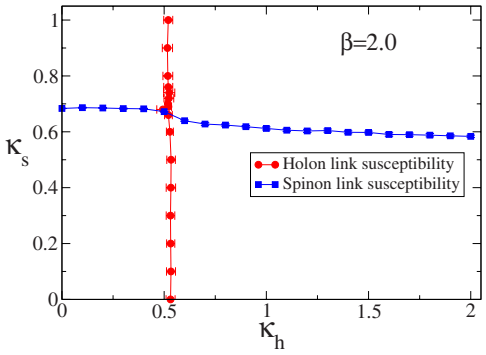

FIG. 11. (Color online) The two-dimensional cross section of the three-dimensional phase diagram (Fig. 9) at $\beta = 2.0$, extracted from a 16^3 lattice using susceptibilities of thermodynamical observables.

The nontrivial signals in the measured susceptibilities indicate the existence of transitions between all four different phases known already from our discussion of the weak coupling limit $\beta \to \infty$, presented in Sec. III. One can clearly observe that at the largest measured β the four different phases meet (within our numerical resolution) in a single crossing point. The numerically observed picture is very similar to the expected behavior in the limit $\beta \to \infty$ as shown in Fig. 8. The horizontal (blue) and vertical (red) phase transitions are of second order, and both belong to the XY universality class. Note that here we do not discriminate between the ordinary and "inverted"[42] universality classes of the XY transitions as they are related by a turnover of the coupling axis, $\kappa \to 1/\kappa$, in the course of a duality transformation.

With decreasing β, the gauge coupling becomes stronger and the phase picture changes (see Fig. 13). Consider first the horizontal transition line which marks the condensation of spinons. At vanishing holon coupling, $\kappa_h = 0$, the phases are separated at a certain "lower border" value (point D) of the critical spinon coupling, $\kappa_s^{\mathrm{crit}}(\kappa_h \to 0, \beta)$, which turns out to be a rapid function of the gauge coupling β. Indeed, as the coupling β decreases, the critical spinon coupling κ_s^{crit} substantially increases. On the other hand, at large values of the holon coupling $\kappa_h \to \infty$, the "upper border" (point B) of the critical spinon coupling $\kappa_s^{\mathrm{crit}}(\kappa_h \to \infty, \beta)$ is practically insensitive to the variation of β.

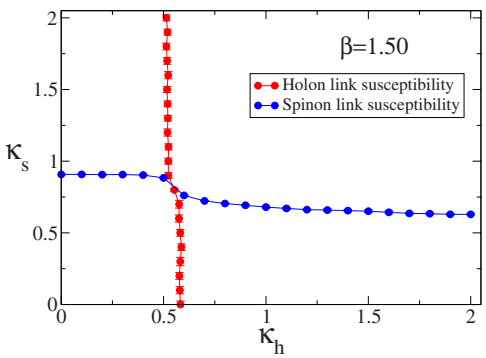

FIG. 12. (Color online) The same as Fig. 11, but for $\beta = 1.5$.

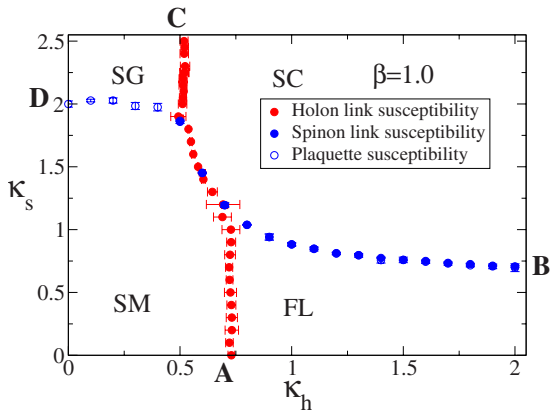

FIG. 13. (Color online) The same as Fig. 11, but for $\beta=1.0$. In addition, the four phases and positions of the points A, B, C, and D of Fig. 9 are explicitly indicated.

The features of evolution of the vertical transition line—which corresponds to the condensation of the holon pairs—is similar to the evolution of the horizontal line. The lower end point of the line (point A) evolves moderately while the upper end point (point C) practically does not move at all. As we have already pointed out in Ref. 21, the indicated line for small κ_s at $\beta=1.0$ near point A no longer belongs to a real phase transition, but characterizes a percolation transition from the SM to the SL phase. This is in agreement with our findings at lower β's discussed below.

It is very interesting to find what happens with these two transition lines in the interior of the phase diagram. As it is already clear from Fig. 12, the two transition lines do not simply cross each other in an isolated point. As the inverse gauge coupling β becomes lower, in the middle of the phase diagram the transition lines become closer and closer to each other in a particular interval of the (κ_s, κ_h) coupling space. The further decrease of the coupling β leads to a qualitative change of the picture in the interior, as it is indicated in Fig. 13: At $\beta=1.0$ the transition lines piecewise join into a single line in a certain (κ_h, κ_s) region. In this region we observe nontrivial signals for a first-order transition in all measured quantities to be discussed in the next section.

In addition to the "thermodynamical observables" (49), the "topological quantities" (densities of defects) also show signals of a phase transition. The density of monopoles ρ_{mon} (at $\beta=1.0$ on a 16^3 lattice) is plotted in the upper panel of Fig. 14 over the (κ_h, κ_s) plane. With increasing hopping parameters κ_h or κ_s the monopole density becomes suppressed. As shown in the middle (lower) panel of Fig. 14 the density of the holon vortices ρ_h (spinon vortices ρ_s) significantly drops down with increasing κ_h (or κ_s, respectively). This behavior is not unexpected because, as one can see from the vortex action (27)–(30), the larger the hopping parameter, the bigger the vortex mass. Therefore, the increase of a particular hopping parameter must suppress the density of the corresponding vortex. As for the monopoles, the increase of either of the hopping parameters should suppress the monopole density because the monopoles are connected by vortices according to Eq. (20) (see the example in Fig. 2). The increase of tension (mass) of either of the vortices leads to

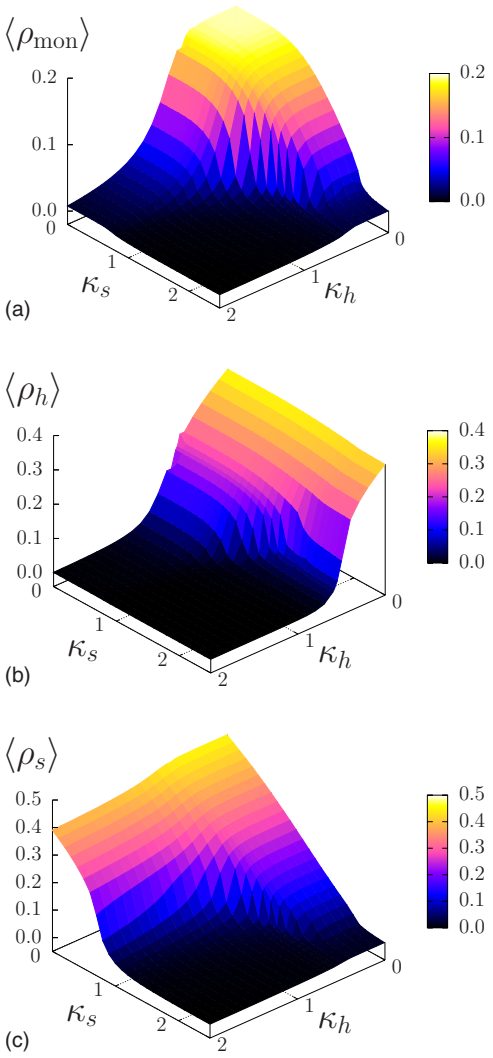

FIG. 14. (Color online) The monopole density (top), the density of holon vortices (middle), and the density of spinon vortices (bottom) at $\beta=1.0$ and 16^3.

the confinement of the monopoles into magnetically neutral monopole-antimonopoles states, and, as a result, this leads to the suppression of the monopole density as we see in Fig. 14 (top). The maximum in the monopole density is seen where both vortex densities are nonzero.

C. Strengthening of the phase transition: "2" + "2" = "1"

The structure of the phase diagram at $\beta > \beta_c^{\mathrm{gI}}$ gives us the possibility to study more in detail the phenomenon of merging (to be distinguished from crossing) of two different independent phase transitions at $\beta \to \infty$ in a finite region of the coupling space.

In order to clarify the nature of the phase transitions, we studied the volume dependence of the average of the plaquette and of both link terms in the action (8) as well as their respective susceptibilities in different regions of the phase diagram. Figure 15 (top) shows the jump developing in the holon link vs κ_h at fixed κ_s with increasing volume. This jump is a clear signal of the first-order nature of the

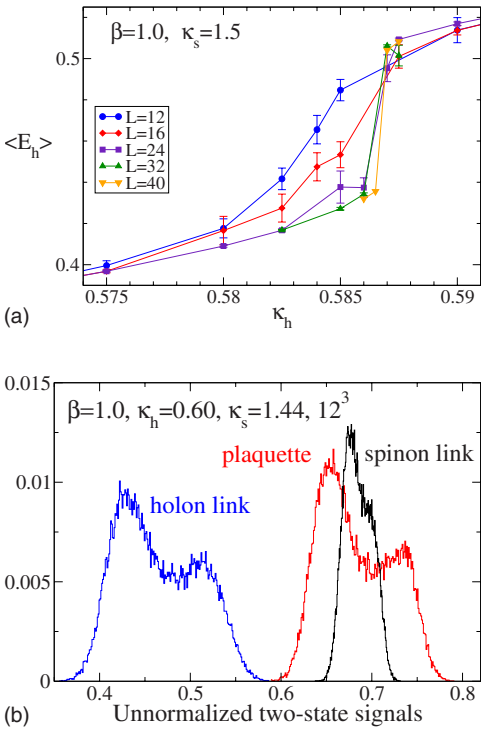

FIG. 15. (Color online) Signatures for the first-order transition at $\beta=1.0$: the holon link expectation value vs κ_h for different volumes at $\kappa_s=1.4$ (top) and (unnormalized) histograms of the parts of the action in the pseudocritical region on a 12^3 lattice (bottom).

transition (it is actually observed in all parts of the action) in the crossing region of the transition lines. Note, however, that a lattice with a size 32^3 turned out to be too large to tunnel for the selected κ_h values, even within 5×10^5 Monte Carlo iterations. The reason is that the free energy barrier for such a large lattice is too high. In Fig. 15 (bottom) we present typical two-state signals (here only for a 12^3 lattice) of all three terms of the action at (κ_h,κ_s) close to the transition. The signals are strong along the *direct transition* line between the SM and SC phases (this line is clearly visible in Fig. 13). The two-state signals of the volume-averaged plaquette and the volume-averaged holon link term become very weak when one goes to smaller κ_h along the joint direct transition between the SM and SC phases in Fig. 13 to the point where the transition lines split. We can conclude that in the crossing region the strength of the new (compared to $\beta=1.5$) direct transition is enhanced compared to the strength of the still separate parts (horizontally and vertically running) of the individual transition lines.

The two-state signals of the volume-averaged plaquette and volume-averaged holon link term become very weak when one goes to smaller κ_h along the horizontal dark-dotted (blue) line. Therefore in the crossing region between the two phases the strength of the phase transition is enhanced compared to the strength of the individual (horizontal and vertical) transition lines. We discuss the order of these transition lines below.

It is known that for $\kappa_h\to0$ the transition vs κ_s is of second order. Similarly, for large κ_h the transition is most likely also of second order, again in the XY universality class. We found

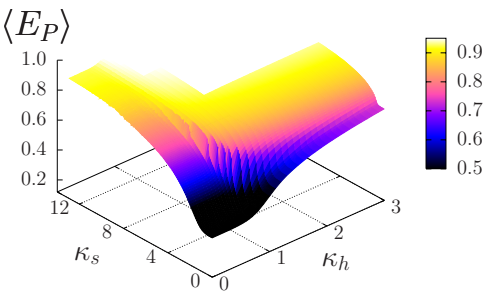

FIG. 16. (Color online) Plaquette expectation value in the (κ_h,κ_s) plane at $\beta=0.8$ on a 16^3 lattice.

that at $\kappa_h=2.0$ already for the largest volumes 40^3–48^3 of our study the increase of the spinon link susceptibility stops as a function of the lattice size. This is the behavior expected for the XY model at $\kappa_h\to\infty$.[43] Concentrating on two κ_s values outside the crossing regime, where one of the transition lines (the light-dotted [red] one) runs vertical, we observe that there is no thermodynamic transition vs κ_h for the smaller κ_s. This is in agreement with what could be anticipated for the limit $\kappa_s\to0$.

Due to the weakness of the signals we were not able to check that, whether for larger but finite values of β (corresponding to weaker gauge coupling), there is still a line of first-order transition somewhere in the region of the phase diagram close to the crossing point. In fact, as β increases, the region in which the two transition lines join tends to shrink. Therefore the properties of the bulk observables—probed by variations of the κ_h hopping parameter—provide a weak signal if the sequence of measurements does not pass through the right (crossing) point at the right (corresponding to a maximal variation of the bulk observables) angle in the coupling space. Anyway, the first-order phase transition should inevitably disappear from the crossing region in the region $\beta\to\infty$ as we surely know from Fig. 8. In short, there is no evidence of a first-order transition outside the merging region.

Increasing further the strength of the gauge coupling (decreasing β below $\beta=1.0$) one should finally approach the critical value of the gauge Ising model, $\beta_c^{\mathrm{gI}}\approx0.7613$, below which the structure of the two-dimensional phase diagram qualitatively changes. In order to see what happens there we studied in detail the cross section of the phase diagram at $\beta=0.8$ which is already very close to the critical value. In Fig. 16 we present the plaquette expectation value $\langle E_P\rangle$ in the (κ_h,κ_s) plane. The white areas in the figure correspond to uninteresting regions in the plane of the couplings at simultaneously large κ_h and κ_s values. From this figure we may expect that the phase transition line corresponding to the spinon condensation is parallel to the κ_h axis for not too small κ_s. The same effect can also be seen in the landscape of the average spinon action $\langle E_s\rangle$ (not shown). Analogously, the holon condensation line is parallel to the κ_s axis for not too small κ_h as can also be seen in the landscape of the average holon action $\langle E_h\rangle$ (not shown).

The maxima of the susceptibilities of the different action contributions demonstrate in more detail the exact location

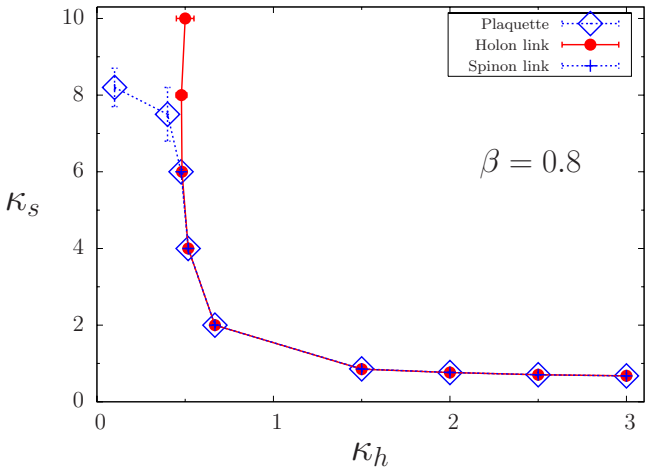

FIG. 17. (Color online) The phase transition lines in the (κ_h, κ_s) plane obtained by searching for peaks of various susceptibilities using multihistogram reweighting for β=0.8 on the 16^3 lattice.

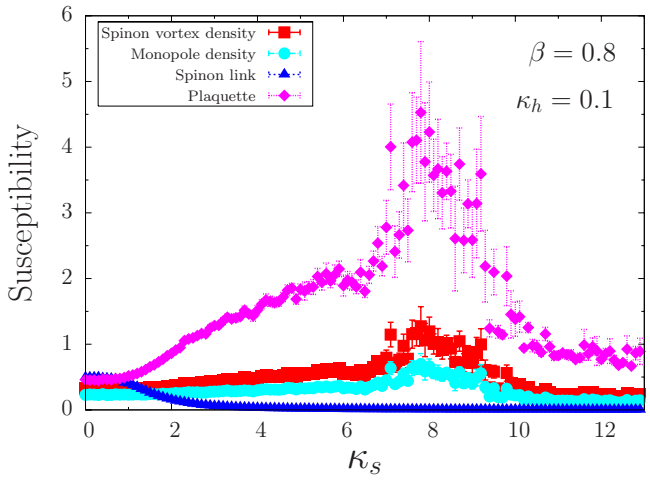

FIG. 18. (Color online) The susceptibilities of thermodynamical and topological quantities at β=0.8, and 16^3 as a function of κ_s at κ_h=0.1.

of the phase transition curves. To obtain accurate pseudocritical couplings we performed several high statistic runs near chosen points indicated in Fig. 17, changing one of the hopping parameters to cross the expected phase transition line.

All obtained Monte Carlo histories of measurements have been evaluated together using a multihistogram reweighting procedure.[44] The combined histograms of observables at a chosen pair of couplings κ_h, κ_s (interpolating among the κ_h, κ_s grid of the used data sets) are obtained by reweighting from the closest data points in the grid. They contain all information necessary to precisely locate the phase transition. In particular, using such a combined histogram interpolating in the range of the chosen hopping parameters we were able to identify the pseudocritical value where the reweighted histogram exhibits a maximum in the susceptibility of the corresponding variable.

To estimate the error in determining the critical couplings, we blocked our original data from several couplings into blocks similar to a jackknife method and constructed individual "subhistograms" at the chosen coupling pair for those data subsets. Using those subhistograms to find the maximum of the susceptibility, different critical couplings have been found which allowed to estimate the accuracy of the location of the critical coupling using all available data.

The results of this detailed investigation is shown in Fig. 17. We used thermodynamical variables in the reweighting as indicated in the legend. Most errors in the pseudocritical couplings are smaller than the symbol sizes, the lines are drawn to guide the eyes.

The individual observables show common signals in certain parts of the phase plane. The region of the common transition line has been increased compared to results at larger β. In addition to the gross structure the susceptibility of the plaquette action shows a weak but measurable signal for the continuation of the "horizontal" line at large $\kappa_s^{\text{crit}} \approx 8.0$ for very small κ_h.

This has been studied in more detail at small κ_h=0.1 in Fig. 18. Weak but relatively sharp signals are observed in some of the susceptibilities shown as functions of the spinon hopping parameter κ_s. Note that contrary to the spinon link susceptibility, a signal is present in the susceptibility of the spinon vortex density. The observed behavior can be interpreted as an indication for the expected second-order phase transition. The spinon-link signal is practically invisible for small κ_h, and it can only be observed at higher values of κ_h. This is a common feature of Fig. 17 and Fig. 13.

The emerging picture is in agreement with our expectation that the critical value of the complementary κ_s should take an infinite value as the value of β approaches the critical coupling β_c^{gI} of the gauge Ising model. Indeed, there is no transition at finite κ_s for the Q=2 Abelian Higgs model at β_c^{gI}.

Figure 17 shows the location of the phase transition lines in a large region of the (κ_h, κ_s) plane. In particular we are convinced that the holon and the spinon-pair condensation lines join for strong gauge couplings just above the gauge Ising model's critical value.

In order to demonstrate that at β=0.8 the phase transition in the merging region is of first order we have considered three different fixed κ_s values, κ_s=2.0, 4.0, and 6.0. In Fig. 19 we present for κ_s=4.0 near criticality nice two-state signals visible in various observables, indicating that the system jumps from one metastable state to another. This is a clear characteristic of a first-order phase transition. The signal is strongest near the center value κ_s=4.0, and then becomes weaker for smaller and larger κ_s values (not shown) where—according to our expectations—the nature of the transition becomes closer to a second-order transition.

The tunnelings between different vacua in the region of the first-order phase transition are clearly visible for small lattice volumes (i.e., 16^3). They can also be seen in the (unnormalized) distribution of the holon energy term shown in Fig. 20 for different lattice volumes and various values of the holon hopping parameter.

The typical features of the first-order phase transition can also be observed, for example, in the behavior of the holon

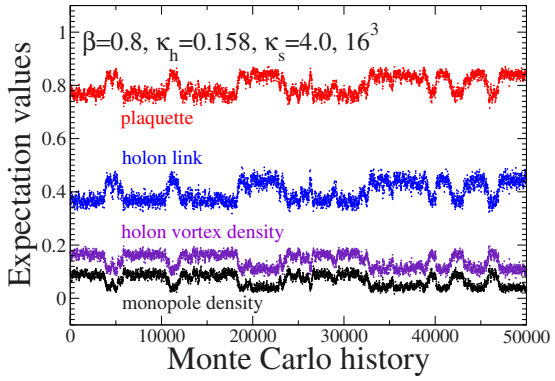

FIG. 19. (Color online) Two-state signals in the Monte Carlo history of several observables near the center (κ_s=4.0) of the merging line of the two transition line as observed at β=0.8 on a 16^3 lattice.

link expectation value. This observable—shown in Fig. 21 as a function of κ_h for the same three chosen values of the hopping parameter κ_s—clearly develops a jump at the phase transition point as the volume of the lattice increases. Thus the model has a nonvanishing latent heat at the phase transition point characterizing a first-order phase transition. The signal of the first order is most clearly visible at κ_s=4.0, while it becomes weaker at larger and smaller values of κ_s in agreement with our observations made with the help of the Monte Carlo histories.

In order to confirm the absence of the phase transition as we expect from either Fig. 10(a) or Fig. 10(c), we investigated the model numerically for a much smaller value of the spinon hopping parameter, κ_s=0.1. The crossover nature of the transition is clear from the susceptibilities of the thermodynamical and topological observables (in Fig. 22): we observe either no susceptibility signal or broad maxima at different values of κ_h. Of course, a remnant of a vortex percolation transition—expected at small κ_s—cannot be ruled out by our investigations and has to be studied using cluster analysis techniques.

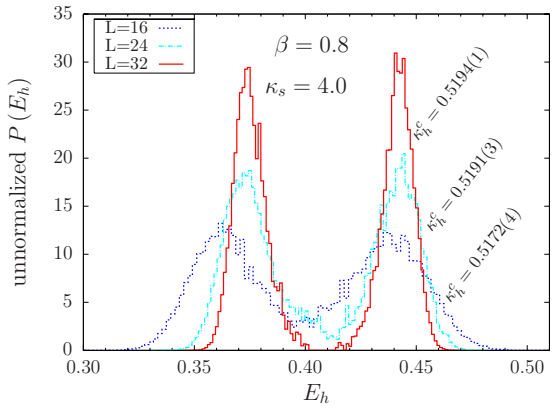

FIG. 20. (Color online) The two-state signal in the histogram of the holon link expectation value E_h=S_h/N_L at β=0.8 and κ_s=4.0 with varying lattice volume reweighted to the transition value κ_h^c at maximal susceptibility.

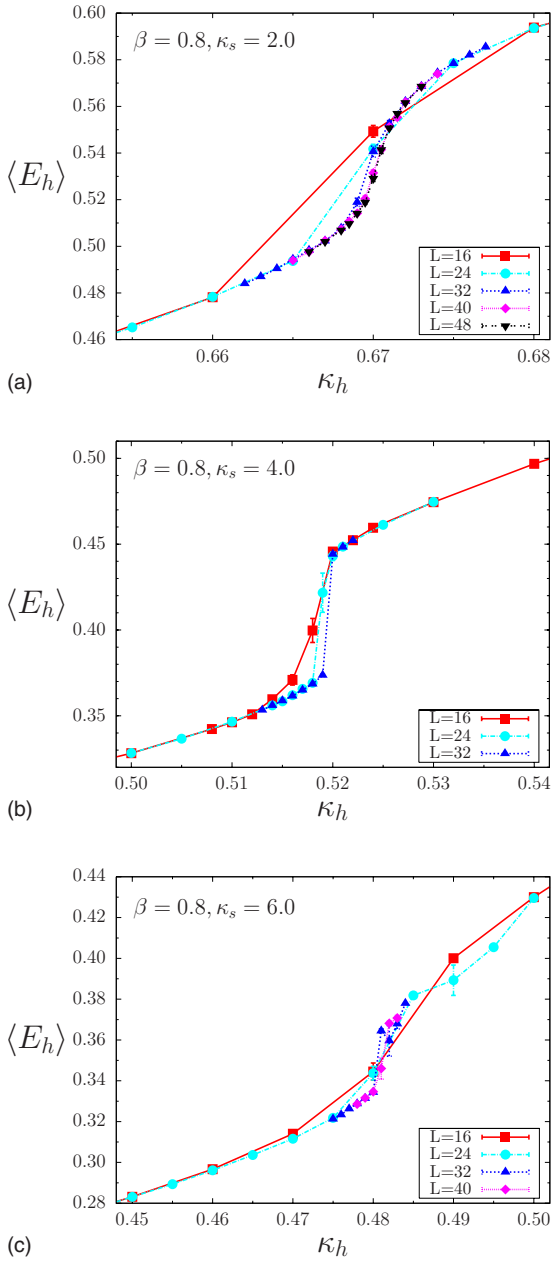

FIG. 21. (Color online) Holon link energy expectation value as a function κ_h for various volumes at β=0.8 for κ_s=2.0 (top), κ_s=4.0 (middle), and κ_s=6.0 (bottom).

Thus, we have strong reasons to conclude that the phase transition scenario at relatively strong gauge coupling, but still above the critical β_c^{gI} of the gauge Ising model, resembles more one of the anticipated scenarios, the phase structure of Fig. 10(a) rather than the closest alternative scenario plotted in Fig. 10(c). Moreover, we have observed that the merged transition in the segment *F*-*G* of Fig. 10(a) has a clearly discontinuous phase transition.

D. The phase structure at strong coupling below β_c^{gI}

In this section we identify the phase structure of the model choosing a really strong gauge coupling, β=0.5

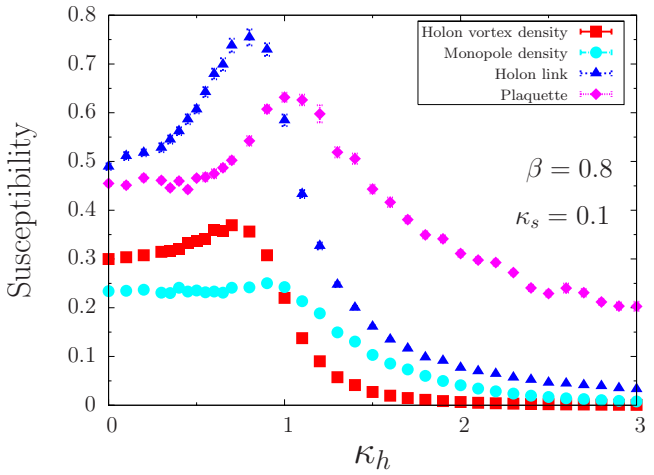

FIG. 22. (Color online) The susceptibilities of thermodynamical and topological quantities at β=0.8, and 16^3 as a function of κ_h at κ_s=0.1.

$< \beta_c^{\mathrm{gl}}$. As in the previous sections we first make an exploratory study of the phase structure for a relatively small lattice size, 16^3.

In Fig. 23 we show the plaquette expectation value and the average densities of all topological defects in the (κ_h, κ_s) plane (for the topological densities the viewpoint is rotated for convenience). Using the gauge degrees of freedom, the approximate phase structure is most easily detected.

It is interesting to discuss the density of the topological defects since they may provide us with the hint how the condensates behave in the different regions of the phase diagram (a condensate is suppressed if the density of the corresponding vortex is nonzero). The density of the holon vortices behaves qualitatively similar to the one in the weak coupling case, Fig. 14. In contrast to this, the density of the spinon vortices is qualitatively different at strong and weak gauge couplings as a function of κ_s and κ_h: while in the weak coupling regime the spinon vortex density rapidly vanishes going to the large-κ_s limit, the same is no longer true in the strong coupling regime. The monopole density is also different in both regimes: in the weak coupling regime the monopole density is visibly nonzero only in the vicinity of the κ_h, κ_s origin, while in the strong coupling regime the monopole density remains almost unaffected towards large values of κ_s. Note that similarly to Fig. 14 the rule remains true that a nonzero monopole density is observed only in the region of the phase diagram where both vortex densities are nonvanishing.

Figures 23 show approximately a structure of the phase diagram qualitatively consistent with our expectations plotted in Fig. 10(b).

In order to study the location of the phase transition line more precisely, we have studied the thermodynamical and topological susceptibilities interpolated by reweighting techniques as for β=0.8. The result of a search for maxima of those susceptibilities is represented in Fig. 24.

We note that the different variables mark a single line in the hopping parameter plane (within our resolution). Signals from the thermodynamical susceptibilities (upper Fig. 24)

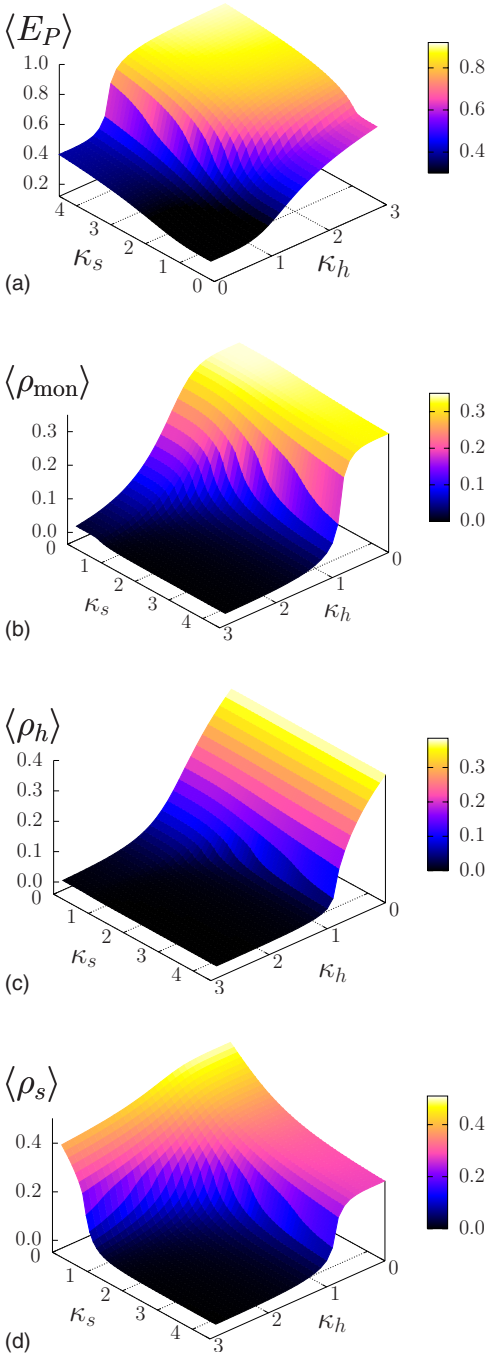

FIG. 23. (Color online) Expectation value of the gauge plaquette and the densities of the topological defects (monopoles, holon vortices, and spinon vortices) at β=0.5 on a 16^3 lattice.

are found in the whole considered (κ_h, κ_s) range. In contrary, using the topological observables (lower Fig. 24), only the maximum of the spinon vertex susceptibility χ_{ρ_s} signals the transition along the whole line. The monopole and holon vertex signals are seen in the common "vertical" line only. It is worth mentioning that the signal in the topological observables is much stronger and clearer compared to the signal of the thermodynamic quantities.

The volume dependence of the susceptibilities of the holon link (top) and the spinon link (bottom) along lines cross-

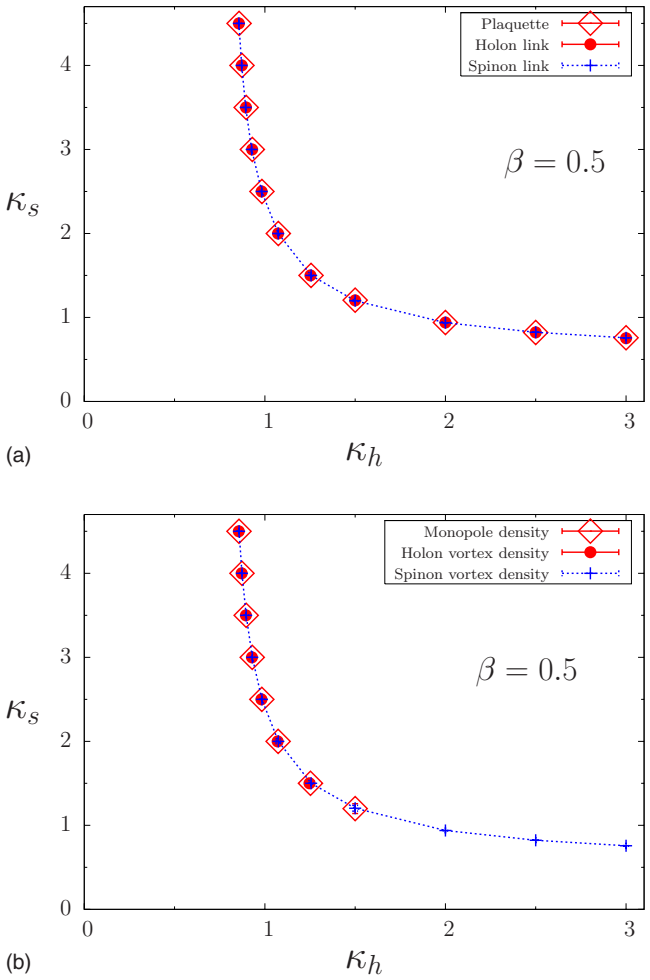

FIG. 24. (Color online) The phase transition line in the (κ_h, κ_s) plane at fixed β=0.5 on the lattice 16^3 to be located by finding the susceptibility peaks of thermodynamical (top) and topological (bottom) variables.

ing the phase transition line horizontally at κ_s=4.0 and vertically at κ_h=3.0 definitely rules out the possibility of a first-order transition (Fig. 25).

Similarly to the weak coupling case $\beta > \beta_c^{\mathrm{gI}}$, a branch of phase transition is absent ranging to very small κ_s=0.1, as it can also be seen from the behavior of various susceptibilities, in Fig. 26. Indeed, these susceptibilities develop non-sharp maxima at significantly different κ_h. Note that the existence of a remnant from a vortex percolation transition cannot be determined by our calculations. It has to be sought for by cluster analysis.

Summarizing this section we mention in short that we observe one main phase transition line which is most presumably of second order. In addition, we see a very weak signal along the vertical line $\kappa_h \sim 1$ for small $\kappa_s \leqslant 1.0$ intersecting the κ_s=0 axis. However, this mentioned signal is not a thermodynamical transition.

The observed picture at β=0.5 is consistent with the phase diagram proposed in Fig. 10(b). We clearly observe the common line *H-B′* indicating the Δ condensation as signaled by the susceptibility maximum of the spinon vortex density and the behavior of the density itself. The "vertical" section

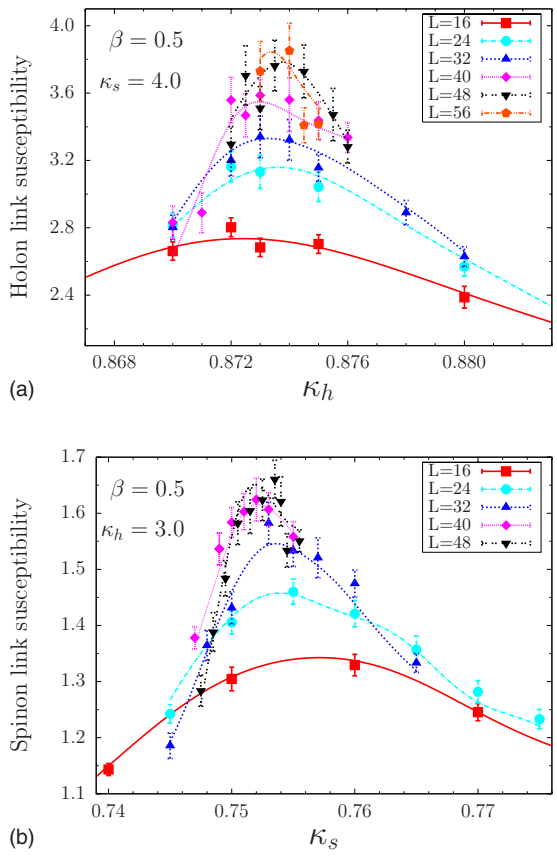

FIG. 25. (Color online) The holon link susceptibility vs κ_h at fixed κ_s=4.0 (top) and the spinon link susceptibility vs κ_s at fixed κ_h=3.0 (bottom) for various lattice volumes at β=0.5 together with the curves obtained by multihistogram reweighting.

H-F′ of the line *H-B′*—showing in addition the *b* condensation—is also present as indicated by the behavior of the holon vortex density.

There is no hint for thermodynamically separated transitions for the condensations. If a line *E-F′* with a point *E* exists, it could be related to percolation properties as can be conjectured from Figs. 23 and 26.

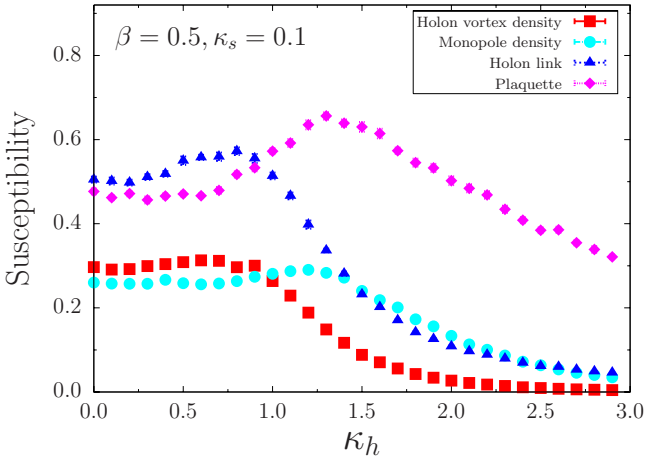

FIG. 26. (Color online) Susceptibilities of thermodynamical and topological quantities vs κ_h at β=0.5, κ_s=0.1, and 16^3.

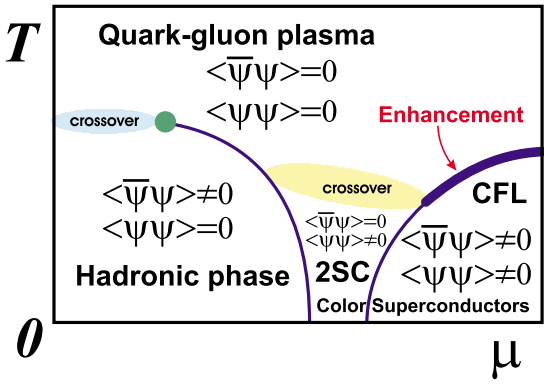

FIG. 27. (Color online) Schematic view of the phase diagram of QCD with a suggested enhancement to a first-order phase transition due to the mediating, strongly coupled gauge field. The explanation is given in the text.

V. THE STRENGTHENING OF PHASE TRANSITIONS AND A POSSIBLE REALIZATION IN QCD

This paper is devoted to the investigation of nontrivial properties of a model containing two Higgs fields coupled to a single compact gauge field. As most remarkable observation we find the possibility that two weak (second-order) phase transitions—marking the vanishing and/or nonvanishing of two different condensates—tend to join and constitute a stronger (first-order) transition at sufficiently strong (but not too strong) gauge coupling. Although the model is related to strongly correlated electron systems in (2+1) dimensions (at zero temperature), we conjecture that the observed effect is much more general such that it can also be realized in the field theory of strong interactions, quantum chromodynamics (QCD). The two-dimensional phase diagram that attracts the attention of lattice theorists and phenomenologists today is spanned by temperature and nonzero baryonic density.

The schematic view of the QCD phase diagram in terms of the baryon chemical potential μ and the temperature T is shown in Fig. 27. For a detailed review we refer to Refs. 45 and 46. The diagram corresponds to QCD with two light quarks (u and d) and one heavier quark (s). The order parameters which are relevant in this phase diagram are the chiral condensate, $\langle\bar{\psi}\psi\rangle$ and the diquark condensate, $\langle\psi\psi\rangle$. It is worth mentioning that due to the presence of three quark flavors the phase structure of the realistic QCD is richer compared to Fig. 27. The structure of the superconducting phases is finer because there are three (instead of one) diquark condensates related to different flavors, and the phases with different combination of nonzero diquark condensates may emerge. A thorough treatment of the QCD phase diagram in an effective model of the quark matter, known as the Nambu-Jona-Lasinio (NJL) model,[47] can be found in Ref. 48. In view of the qualitative character of our considerations we ignore the color, flavor, and Dirac indices in the notation, and we do not discriminate between different quark flavors taking the schematic picture shown in Fig. 27 as a reference point.

At low temperature and density, strongly interacting matter is in the hadronic phase which is characterized by broken chiral and unbroken color symmetries, so that the quark condensate is nonvanishing while the diquark condensate vanishes. As temperature increases, matter goes over into the quark-gluon plasma (QGP) phase in which both condensates vanish. At small chemical potential the transition between these phases is probably a smooth crossover[49] rather than a real phase transition, so that in this region the difference between the two phases is marginal (and the vanishing of $\langle\bar{\psi}\psi\rangle$ is not complete). However, the chiral condensate is drastically suppressed in the high temperature regime, what we formally express in Fig. 27 by $\langle\bar{\psi}\psi\rangle=0$. We adopt the same convention for other exponentially suppressed but nonvanishing condensates. The phases on both sides of a crossover are often said to be connected via an analytical continuation. Consequently, in a strict mathematical sense, the chiral condensate does not take zero value at any point of the quark-gluon plasma phase.

As the chemical potential increases, the crossover between the hadron and the QGP phases turns into a second-order transition denoted by a dot in Fig. 27. The second-order phase transition is an endpoint of a first-order phase transition line that separates the hadronic phase not only from the QGP phase but also from one of the color superconducting phases, the so-called 2SC phase, in which two colors are locked with the global flavor symmetries through the formation of a nonzero diquark condensate, $\langle\psi\psi\rangle\neq 0$. Note that in the 2SC phase the chiral condensate is zero.[45]

The 2SC phase is presumably also separated by a crossover from the QGP phase and by a first order phase transition from another color superconducting phase in which all three colors are locked with all three flavor degrees of freedom (this phase is known as "color-flavor locked," or CFL, phase). The CFL phase is the only phase where both chiral and diquark condensates are simultaneously nonvanishing.[45] In Ref. 50 it is demonstrated that the transition between the QGP and the CFL phase must be of first order due to the thermal fluctuations of the gauge field.

Needless to say that the system of strongly interacting gluons coupled to dynamical quarks in (3+1) dimensions is much more complicated than a simplified gauge model of correlated electrons in (2+1) dimensions. However, there are some qualitative similarities between these theories as far as the structure of the phase diagram is concerned comparing, say, Fig. 10(a) with Fig. 27. The compact Abelian two-Higgs model may be realized in one of four different phases: Fermi liquid, spin gap, strange metal, and superconducting phases which are characterized by pairs of vanishing or nonvanishing condensates (b or holon, Δ or spinon-pair condensates, see also Fig. 1). The QCD phases can also be characterized by a pair of quark and diquark condensates $(\langle\bar{\psi}\psi\rangle,\langle\psi\psi\rangle)$. According to Fig. 13, an enhancement of the strength of the phase transition may take place (at sufficiently strong gauge coupling) where both condensates simultaneously change from vanishing to nonvanishing. The same pattern is realized in QCD between the CFL phase and the QGP phase. The corresponding segment of the phase transition is the result of joining two "transitions," the crossover transition between

the 2SC color superconductor and the QGP on one hand and the first order phase transition between the 2SC phase and the CFL phase.

Our experience with the cA2HM suggests that such a merging of two weaker transitions—provided they separate the phase characterized by simultaneously vanishing condensates from the phase with all condensates nonvanishing—may lead to an enhancement of the order compared to the strength of the individual transition lines. Therefore we expect that the finite-temperature transition between the CFL and the QGP phases—except for very large baryon density where the coupling should become weaker due to asymptotic freedom—would be much stronger than between the 2SC and the CFL superconducting phases taking place at lower temperature and chemical potential.

As we have discussed above, the key ingredient of the transition strengthening in the effective model of the strongly correlated electrons is a gauge-boson mediated interaction between the species of the matter fields. As a result, the transition in different channels and/or species merge and the merger corresponds to a much stronger phase transition. The strengthening effect cannot be seen in QCD phase diagram studies using the effective NJL model of quark matter (see, for example, Ref. 48) because that model possesses global symmetries only and the gauge field mediation is obviously absent. There are, in fact, indications[50] that in QCD the thermal fluctuations of the gauge fields strengthen the first order phase transition between the QGP and CFL phases, which nicely matches with our qualitative expectation.

VI. CONCLUSIONS

In this paper we have studied in detail the phase diagram of the $(2+1)D$ Abelian Higgs model with two Higgs fields and one compact gauge field. At weak gauge coupling (large β) the phase diagram contains two transition lines which run through the whole plane in the hopping parameter (κ_h, κ_s) plane. The transitions are associated with the onset of vortex percolation, and with the appearances of holon and spinon-pair condensates. The pattern of nonvanishing condensates in different regions of the phase diagram allows to identify the Fermi liquid, spin gap, superconductor, and strange metallic phases.

With decreasing β above the critical coupling of the gauge-Ising model the strange metallic and Fermi liquid phases become analytically connected at small κ_s, eventually still being separated by a percolation transition.

At extremely strong coupling (with β below the gauge-Ising model transition), however, one of the segments of the transitions disappears together with the spin gap phase, while the difference between the strange metal and the Fermi liquid phases becomes almost invisible since these phases are separated by a smooth crossover in this limit.

The most intriguing effect—which was first suggested in Ref. 21—is a strong enhancement of the strength of the phase transition. This enhancement appears in the regime of moderately strong gauge coupling in which the two second-order transitions—corresponding to spinon-pair and holon condensation lines–join. The enhancement happens along the common segment of the phase transition and is reflected in lowering the transition order: two second-order transitions become a single first order transition between the two phases where the two condensates are both vanishing and both nonvanishing. That strengthening comes as a result of a coherent dynamics of both condensates coupled together by the internal gauge field. In fact, the reason of the merging and subsequent enhancement of the transitions in this particular model must be due to the dynamics of the compact gauge field since it is only the gauge field which couples both scalar fields with each other. The compact gauge field possesses topological magnetic defects which are especially dense in the strong gauge coupling region. Given the fact that the merging region widens as the gauge coupling becomes stronger, we suggest that the monopole dynamics may be held responsible for merging and subsequent strengthening of the phase transitions.

We suggest that a similar enhancement effect may also be realized in quantum chromodynamics at nonzero temperature and at finite baryon density. At sufficiently large baryon density the finite-temperature transition between the (three-flavor paired) color superconducting phase and the quark-gluon plasma phases should be much stronger compared with the transition between two-flavor paired and three-flavor paired superconducting phases. The suggested enhancement is emphasized in Fig. 27.

ACKNOWLEDGMENTS

E.-M.I. is supported by the DFG Forschergruppe 465 "Gitter-Hadronen-Phänomenologie." M.N.C. is supported by Grants No. RFBR 05-02-16306a, No. RFBR-DFG 06-02-04010, and by a STINT Institutional Grant No. IG2004-2 025. M.N.C. wishes to thank I. Ichinose, T. Matsui, and J.J.M. Verbaarschot for illuminating discussions. M.N.C. is also grateful to the members of the Department of Theoretical Physics at Uppsala University for the kind hospitality and stimulating environment.

[1] J. Smiseth, E. Smorgrav, and A. Sudbo, Phys. Rev. Lett. **93**, 077002 (2004); E. Smorgrav, J. Smiseth, E. Babaev, and A. Sudbo, *ibid.* **94**, 096401 (2005); J. Smiseth, E. Smorgrav, E. Babaev, and A. Sudbo, Phys. Rev. B **71**, 214509 (2005).

[2] E. Babaev, A. Sudbo, and N. W. Ashcroft, Nature (London) **431**, 666 (2004); E. Babaev, L. D. Faddeev, and A. J. Niemi, Phys. Rev. B **65**, 100512(R) (2002); E. Babaev, Phys. Rev. Lett. **89**, 067001 (2002).

[3] T. Senthil, L. Balents, S. Sachdev, A. Vishwanath, and M. P. A. Fisher, Phys. Rev. B **70**, 144407 (2004); S. Sachdev, in *Quantum Magnetism*, edited by U. Schollwock, J. Richter, D. J. J. Farnell, and R. A. Bishop, Lecture Notes in Physics (Springer,

Berlin, 2004).
[4] P. A. Lee, N. Nagaosa, and X.-G. Wen, Rev. Mod. Phys. **78**, 17 (2006).
[5] T. Ono, Y. Moribe, S. Takashima, I. Ichinose, T. Matsui, and K. Sakakibara, Nucl. Phys. B **764**, 168 (2007); T. Ono and I. Ichinose, Phys. Rev. B **74**, 212503 (2006).
[6] P. W. Anderson, *The Theory of Superconductivity in the High-T_c Cuprate Superconductors* (Princeton University Press, Princeton, NJ, 1997).
[7] E. Dagotto, Rev. Mod. Phys. **66**, 763 (1994); P. W. Anderson, M. Randeria, T. Rice, N. Trivedi, and F. Zhang, J. Phys.: Condens. Matter **16**, R755 (2004).
[8] D. N. Basov and T. Timusk, Rev. Mod. Phys. **77**, 721 (2005); F. Gervais, Mater. Sci. Eng., R. **39**, 29 (2002).
[9] P. W. Anderson, Science **235**, 1196 (1987); F. C. Zhang and T. M. Rice, Phys. Rev. B **37**, R3759 (1988).
[10] S. E. Barnes, J. Phys. F: Met. Phys. **6**, 1375 (1976); P. Coleman, Phys. Rev. B **29**, 3035 (1984); X. G. Wen, F. Wilczek, and A. Zee, *ibid.* **39**, 11413 (1989); C. Mudry and E. Fradkin, *ibid.* **49**, 5200 (1994).
[11] G. Baskaran, Z. Zou, and P. W. Anderson, Solid State Commun. **63**, 973 (1987).
[12] G. Baskaran and P. W. Anderson, Phys. Rev. B **37**, R580 (1988).
[13] L. B. Ioffe and A. I. Larkin, Phys. Rev. B **39**, 8988 (1989); L. B. Ioffe and G. Kotliar, *ibid.* **42**, 10348 (1990).
[14] M. N. Chernodub and A. J. Niemi, Pis'ma Zh. Eksp. Teor. Fiz. **85**, 435 (2007).
[15] L. D. Faddeev and A. J. Niemi, Phys. Lett. B **464**, 90 (1999); A. J. Niemi and N. R. Walet, Phys. Rev. D **72**, 054007 (2005); A. J. Niemi, AIP Conf. Proc. **806**, 114 (2006); M. N. Chernodub, Phys. Lett. B **637**, 128 (2006).
[16] N. Nagaosa and P. A. Lee, Phys. Rev. B **45**, 966 (1992); P. A. Lee and N. Nagaosa, *ibid.* **46**, 5621 (1992).
[17] N. Nagaosa and P. A. Lee, Phys. Rev. B **61**, 9166 (2000).
[18] I. Ichinose and T. Matsui, Phys. Rev. B **51**, 11860 (1995); I. Ichinose, T. Matsui, and M. Onoda, *ibid.* **64**, 104516 (2001).
[19] G. Baskaran, Indian J. Phys. **89**, 583 (2006); arXiv:cond-mat/0611548 (unpublished).
[20] C. M. Varma, Phys. Rev. B **55**, 14554 (1997); C. Castellani, C. D. Castro, and M. Grilli, Z. Phys. B: Condens. Matter **103**, 137 (1997); J. L. Tallon and J. W. Loram, Physica C **349**, 53 (2000).
[21] M. N. Chernodub, E.-M. Ilgenfritz, and A. Schiller, Phys. Rev. B **73**, 100506(R) (2006).
[22] S. Kragset, E. Smorgrav, J. Hove, F. S. Nogueira, and A. Sudbo, Phys. Rev. Lett. **97**, 247201 (2006); A. Kuklov, N. Prokof'ev, B. Svistunov, and M. Troyer, Ann. Phys. (N.Y.) **321**, 1602 (2006); T. Ono, I. Ichinose, and T. Matsui, arXiv:0704.1323 (unpublished).
[23] J. Villain, J. Phys. (France) **36**, 581 (1975).
[24] A. H. Guth, Phys. Rev. D **21**, 2291 (1980); P. Becher and H. Joos, Z. Phys. C **15**, 343 (1982); a review can be found by M. N. Chernodub and M. I. Polikarpov, in *Confinement, Duality, and Nonperturbative Aspects of QCD*, edited by Pierre Van Baal (Plenum, New York, 1998).
[25] V. L. Berezinsky, Sov. Phys. JETP **32**, 493 (1971); J. M. Kosterlitz and D. J. Thouless, J. Phys. C **6**, 1181 (1973).
[26] A. M. Polyakov, Nucl. Phys. B **120**, 429 (1977).
[27] E. Fradkin and S. H. Shenker, Phys. Rev. D **19**, 3682 (1979).
[28] K. Osterwalder and E. Seiler, Ann. Phys. **110**, 440 (1978).
[29] M. B. Einhorn and R. Savit, Phys. Rev. D **17**, 2583 (1978); **19**, 1198 (1979).
[30] M. N. Chernodub, E.-M. Ilgenfritz, and A. Schiller, Phys. Lett. B **547**, 269 (2002).
[31] J. Kertész, Physica A **161**, 58 (1989).
[32] S. Wenzel, E. Bittner, W. Janke, A. M. J. Schakel, and A. Schiller, Phys. Rev. Lett. **95**, 051601 (2005); PoS (LAT2005) 248 (2006).
[33] M. N. Chernodub, F. V. Gubarev, E.-M. Ilgenfritz, and A. Schiller, Phys. Lett. B **443**, 244 (1998); M. N. Chernodub, Phys. Rev. Lett. **95**, 252002 (2005); Z. Nussinov, Phys. Rev. D **72**, 054509 (2005).
[34] A. P. Gottlob and M. Hasenbusch, Physica A **201**, 593 (1993); G. Kohring, R. E. Shrock, and P. Wills, Phys. Rev. Lett. **57**, 1358 (1986).
[35] R. D. Sedgewick, D. J. Scalapino, and R. L. Sugar, Phys. Rev. B **65**, 054508 (2002).
[36] F. J. Wegner, J. Math. Phys. **12**, 2259 (1971); R. Balian, J. M. Drouffe, and C. Itzykson, Phys. Rev. D **11**, 2098 (1975).
[37] V. Agostinia, G. Carlinoa, M. Caselle, and M. Hasenbusch, Nucl. Phys. B **484**, 331 (1997); M. Caselle and M. Hasenbusch, *ibid.* **470**, 435 (1996).
[38] T. Senthil and M. P. A. Fisher, Phys. Rev. B **62**, 7850 (2000); O. I. Motrunich and T. Senthil, Phys. Rev. Lett. **89**, 277004 (2002).
[39] J. Smiseth, E. Smorgrav, F. S. Nogueira, J. Hove, and A. Sudbo, Phys. Rev. B **67**, 205104 (2003).
[40] M. N. Chernodub, R. Feldmann, E.-M. Ilgenfritz, and A. Schiller, Phys. Rev. D **71**, 074502 (2005); Phys. Lett. B **605**, 161 (2005).
[41] M. N. Chernodub, M. I. Polikarpov, and M. A. Zubkov, Nucl. Phys. B, Proc. Suppl. **34**, 256 (1994).
[42] C. Dasgupta and B. I. Halperin, Phys. Rev. Lett. **47**, 1556 (1981).
[43] M. Campostrini, M. Hasenbusch, A. Pelissetto, P. Rossi, and E. Vicari, Phys. Rev. B **63**, 214503 (2001).
[44] A. M. Ferrenberg and R. H. Swendsen, Phys. Rev. Lett. **63**, 1195 (1989).
[45] Mark Alford, Annu. Rev. Nucl. Part. Sci. **51**, 131 (2001).
[46] M. Stephanov, PoS (LAT2006) 024 (2006).
[47] Y. Nambu and G. Jona-Lasinio, Phys. Rev. **122**, 345 (1961).
[48] S. B. Ruster, V. Werth, M. Buballa, I. A. Shovkovy, and D. H. Rischke, Phys. Rev. D **72**, 034004 (2005); D. Blaschke, S. Fredriksson, H. Grigorian, A. M. Oztas, and F. Sandin, *ibid.* **72**, 065020 (2005).
[49] Y. Aoki, G. Endrodi, Z. Fodor, S. D. Katz, and K. K. Szabo, Nature (London) **443**, 675 (2006).
[50] T. Matsuura, K. Iida, T. Hatsuda, and G. Baym, Phys. Rev. D **69**, 074012 (2004); I. Giannakis, D. Hou, H. C. Ren, and D. H. Rischke, Phys. Rev. Lett. **93**, 232301 (2004); S. Digal, T. Hatsuda, and M. Ohtani, arXiv:hep-lat/0511018, in Proceedings of the Workshop on Extreme QCD, edited by G. Aarts and S. Hands (University of Wales, Swansea, 2006); J. L. Noronha, H. C. Ren, I. Giannakis, D. Hou, and D. H. Rischke, Phys. Rev. D **73**, 094009 (2006).